Transition and Laminar Instability

Transition and Laminar Instability

Leslie M. Mack

May 15, 1977

PREFACE

The work described in this report was performed by the Earth and Space Sciences Division of the Jet Propulsion Laboratory.

This report is Chapter 3 of <u>Application and Fundamentals of Turbulence</u>, to be published by Plenum Press of London and New York. The report was presented as a Short Course Lecture at the University of Tennessee Space Institute, Tullahoma, Tennessee, on January 11, 1977.

ACKNOWLEDCEMENT

TABLE OF CONTENTS

FIGURES

ABSTRACT

A review is given of the application of linear stability theory to
the problem of boundary-layer transition in incompressible flow. The theory
is put into a form suitable for three-dimensional boundary layers; both the
temporal and spatial theories are examined; and a generalized Gaster rela-
tion for three-dimensional boundary layers is derived. Numerical examples
include the stability characteristics of Falkner-Skan boundary layers, the
accuracy of the two-dimensional Gaster relation for these boundary layers,
and the magnitude and direction of the group velocity for oblique waves in
the Blasius boundary layer. A review is given of the available experiments
which bear on the validity of stability theory and its relation to transition.
The final section is devoted to the application of stability theory to tran-
sition prediction. Liepmann's method, the e^n method, and the modified e^n
method, where n is related to the external disturbance level, are all dis-
cussed. A different type of method, called the amplitude method, is described
in which the wide-band disturbance amplitude in the boundary layer is esti-
mated from stability theory and an interaction relation for the initial ampli-
tude density of the most unstable frequency. This method is applied to the
effect of freestream turbulence on the transition of Falkner-Skan boundary
layers.

I. HISTORICAL BACKGROUND

The earliest explanation for the appearance of turbulence was that the laminar flow becomes unstable, and the linear stability theory was first developed to explore this possibility. A series of papers by Rayleigh[1] provided many notable results concerning the instability of inviscid flows, such as inflectional instability, but little progress was made toward the original goal. Viscosity was commonly thought to act only to stabilize the flow, but in 1921 Prandtl[2] showed that viscosity can also be destabilizing. It was this discovery that finally provided a mechanism for the instability of boundary layers in zero and favorable pressure gradients which are stable to purely inviscid disturbances. However, it was not until some years later that Tollmien[3] worked out a complete theory of boundary-layer stability, and for the first time computed a meaningful critical Reynolds number (Re_{cr}), i.e. the lowest Reynolds number at which instability appears. Any expectation that instability and transition to turbulence are synonymous in boundary layers was dashed by the low value of Re_{cr} for the flat-plate boundary layer. Tollmien's calculation gave a value of 420 for the critical displacement-thickness Reynolds number, which is equivalent to $Re_{cr} = U_1^* x^* / v^* = 6 \times 10^4$. Even in the high turbulence level wind tunnels of that time, transition was found between $Re_t = 3.5 \times 10^5$ and 1×10^6.

In what can be considered the earliest application of linear stability theory to transition prediction, Schlichting[4] calculated the amplitude ratio A/A_0 of the most amplified frequency as a function of Reynolds number for a flat-plate boundary layer, and found that this quantity had values between five and nine at the observed transition Reynolds numbers. Outside of Germany, the stability theory received little acceptance because of failure to

observe the predicted waves, mathematical difficulties, and also the feeling that a linear theory could not have much to say about the origin of turbulence which is inherently non-linear. The experiment of Schubauer and Skramstad[5] completely revised this opinion, and unequivocally demonstrated the existence of instability waves in a boundary layer, their connection with transition, and the quantitative description of their behavior by the theory of Tollmien and Schlichting. This experiment made an enormous impact at the time of its publication, and by its very completeness seemed to answer most questions concerning the linear theory. To a large extent, subsequent experimental work on transition went in other directions, and the possibility that linear theory can be quantitatively related to transition has not received a decisive experimental test. On the other hand, it is generally accepted that flow parameters such as pressure gradient, suction and heat transfer qualitatively affect transition in the manner predicted by stability theory, and in particular that a flow predicted to be stable by the theory should remain laminar. This expectation has often been deceived. A good introduction into the complexity of transition and the difficulties involved in trying to arrive at a rational approach to its prediction can be found in a report by Morkovin.[6]

Investigators in Germany applied the stability theory to boundary layers with pressure gradients and suction, and this work is summarized in Schlichting's book.[7] We may make particular mention of Pretsch's[8] work, as he provided the only large body of numerical results for exact boundary-layer solutions before the advent of the computer age by calculating the stability characteristics of the Falkner-Skan family of velocity profiles. The mathematics of the asymptotic theory were put on a firmer foundation by Lin,[9] and this work has

been continued by Reid.[10] When in about 1960 the digital computer reached a stage of development permitting the direct numerical solution of the primary differential equations, the linear theory was extended to many more boundary-layer flows: three-dimensional boundary layers (Brown[11]); free-convection boundary layers (Kurtz and Crandall[12] and Nachtsheim[13]); compressible boundary layers (Brown[14] and Mack[15]); boundary layers on compliant walls (Landahl and Kaplan[16]); a recomputation of the Falkner-Skan flows (Wazzan, Okamura, and Smith[17]); a quasi-steady calculation of unsteady boundary layers (Obremski, Morkovin, and Landahl[18]); and heated-wall water boundary layers (Wazzan, Okamura, and Smith[19]).

It will be the main purpose of this chapter to explain in detail the use of linear stability theory as a means of transition prediction. Enough of the theory is presented in Section II to make it clear how the essential quantity, the amplitude ratio A/A_o, is obtained. The use of temporal and spatial amplification theories is discussed, and a numerical procedure presented which allows eigenvalues to be calculated to arbitrarily high Reynolds numbers. A few numerical examples are given, and in Section III the available experiments bearing on stability theory are examined. Finally, in Section IV the application of linear theory to transition prediction is taken up, and the e^9, modified e^9 and amplitude methods are discussed and applied to the effect of freestream turbulence on transition. It must be emphasized that the subject matter is restricted to incompressible boundary layers along an impermeable surface of zero curvature in the absence of body forces. Görtler instability, free shear flows, and stratified, rotating and compressible flows, are all excluded.

Before proceeding further, it is well to mention some general references. These are review articles on stability theory by Schlichting[20], Shen[21],

Stuart[22] and Reid[23]; and books by Lin[24] and Betchov and Criminale.[25]
Schlichting's[7] book on boundary-layer theory contains two chapters on stability
and transition, and Monin and Yaglom's[26] book on turbul nce contains a single
lengthy chapter on the same subject, as does the book by White[27] on viscous
flow theory. Reviews of transition have been given by Dryden,[28] Tani,[29]
Morkovin[6] and Reshotko.[30] An extensive discussion of both stability theory
and transition, not all at high speeds in spite of the title, may be found in
the Morkovin-Mack recorded lectures.[31]

II. STABILITY THEORY

A. Formulation of Eigenvalue Problem

1. Derivation of Equations

The stability theory starts with the time dependent Navier-Stokes
equations, not the boundary-layer equations. We will restrict ourselves to
the flow of a single incompressible fluid on a surface of negligible curvature.
This simplification eliminates many possible sources of instability, but
preserves the two which are essential to an understanding of the subject:
inflectional and viscous instability. The Navier-Stokes equations for a
viscous incompressible fluid in Cartesian coordinates are

$$\frac{\partial u}{\partial t} + u \frac{\partial u}{\partial x} + v \frac{\partial u}{\partial y} + w \frac{\partial u}{\partial z} = -\frac{1}{\rho} \frac{\partial p}{\partial x} + \nu \nabla^2 u, \tag{1}$$

$$\frac{\partial v}{\partial t} + u \frac{\partial v}{\partial x} + v \frac{\partial v}{\partial y} + w \frac{\partial v}{\partial z} = -\frac{1}{\rho} \frac{\partial p}{\partial y} + \nu \nabla^2 v, \tag{2}$$

$$\frac{\partial w}{\partial t} + u \frac{\partial w}{\partial x} + v \frac{\partial w}{\partial y} + w \frac{\partial w}{\partial z} = -\frac{1}{\rho} \frac{\partial p}{\partial z} + \nu \nabla^2 w, \tag{3}$$

$$\frac{\partial u}{\partial x} + \frac{\partial v}{\partial y} + \frac{\partial w}{\partial z} = 0. \tag{4}$$

The x-axis is in the direction of the freestream velocity, the y axis is normal to the surface, and the z axis is normal to the x and y axes. The velocities u, v, w are in the x, y, z directions, respectively. The density is ρ, the pressure p, and the kinematic viscosity coefficient $\nu = \mu/\rho$. The first three equations are the x, z, z momentum equations; the fourth equation is the equation of continuity.

All flow quantities are divided into a steady mean-flow term and an unsteady fluctuation term. A typical term is

$$q(x,y,z,t) = Q(x,y,z) + q'(x,y,z,t). \tag{5}$$

The mean-flow terms satisfy the boundary-layer equations. When expressions similar to (5) are substituted into (1)-(4) for all flow variables, the mean-flow terms dropped which are negligible by the boundary-layer equations, the mean boundary-layer equations subtracted out, and the nonlinear terms neglected, a much simplified, but still too complicated, system of equations results. The additional assumption of locally parallel flow,

$$U = U(y), \quad W = W(y), \quad V = 0, \tag{6}$$

reduces the equations sufficiently so that upon the introduction of a sinusoidal disturbance they become ordinary differential equations.

The parallel-flow equations are, in dimensionless form,

$$\frac{\partial u'}{\partial t} + U\frac{\partial u'}{\partial x} + W\frac{\partial u'}{\partial z} + v'\frac{dU}{dy} = -\frac{1}{\rho}\frac{\partial p'}{\partial x} + \frac{1}{R}\nabla^2 u', \tag{7}$$

$$\frac{\partial v'}{\partial t} + U\frac{\partial v'}{\partial x} + W\frac{\partial v'}{\partial z} = -\frac{1}{\rho}\frac{\partial p'}{\partial y} + \frac{1}{R}\nabla^2 v', \tag{8}$$

$$\frac{\partial w'}{\partial t} + U \frac{\partial w'}{\partial x} + W \frac{\partial w'}{\partial z} + v' \frac{dW}{dy} = -\frac{1}{\rho} \frac{\partial p'}{\partial z} + \frac{1}{R} \nabla^2 w', \tag{9}$$

$$\frac{\partial u'}{\partial x} + \frac{\partial v'}{\partial y} + \frac{\partial w'}{\partial z} = 0. \tag{10}$$

From now until Section IV dimensional quantities will be denoted by asterisks. The velocity scale is the freestream velocity U_1^*, the length scale is L^* (left unspecified for the present), and the pressure scale ρU_1^{*2}. The Reynolds number is

$$R = U_1^* L^* / \nu^*. \tag{11}$$

These equations, which are the basis of almost all stability investigations, are exact for the flow in a channel or for Couette flow, but are only an approximation for boundary-layer flows. If the multiple scale or two-timing method first applied to this problem by Bouthier[32] and later by Saric and Nayfeh[33] is used, the above equations appear as the zeroth approximation. The next approximation takes the growth of the boundary layer into account. Although this method may be desirable for refined calculations, it is not needed for an elementary presentation of the subject and will not be pursued here.

2. Introduction of Sinusoidal Disturbances

The final form of the differential equations, where the coefficients are functions only of y, and x, z, t appear only as derivatives, suggests the following type of disturbance:

$$(u',v',w',p') = (f,\phi,h,\pi) \exp \left[i(\alpha x + \beta z - \omega t) \right]. \tag{12}$$

Here, $f(y)$, $\phi(y)$, $h(y)$, $\pi(y)$ are the complex amplitude functions of the disturbance flow variables u', v', w', p'; α and β are the dimensionless wave numbers $2\pi L^*/\lambda_x^*$ and $2\pi L^*/\lambda_z^*$, where λ_x^* and λ_z^* are the wavelengths in the x and z directions, respectively, and ω is the dimensionless frequency $\omega^* L^*/U_1^*$. For the moment, α, β, ω may be either real or complex.

When (12) is substituted into (7)-(10), the following equations for the amplitude function are obtained:

$$i(\alpha U + \beta W - \omega)\, f + U'\phi = - i\alpha\pi + \frac{1}{R} [f'' - (\alpha^2 + \beta^2)\, f], \tag{13}$$

$$i(\alpha U + \beta W - \omega)\, \phi = - \pi' + \frac{1}{R} [\phi'' - (\alpha^2 + \beta^2)\phi], \tag{14}$$

$$i(\alpha U + \beta W - \omega)\, h + W'\phi = - i\beta\pi + \frac{1}{R} [h'' - (\alpha^2 + \beta^2)\, h], \tag{15}$$

$$i(\alpha f + \beta h) + \phi' = 0. \tag{16}$$

The primes now refer to differentiation with respect to y. The boundary conditions are that the no-slip condition applies at the wall,

$$f(0) = 0, \quad \phi(0) = 0, \quad h(0) = 0, \tag{17}$$

and that the disturbances go to zero (or are at least bounded) as $y \to \infty$,

$$f(y) \to 0, \quad \phi(y) \to 0, \quad h(y) \to 0 \text{ as } y \to \infty. \tag{18}$$

Since all of the boundary conditions are homogeneous, it can be expected that solutions to (13)-(16) will exist only for particular combinations of R, α, β,

and ω. Consequently, we have an eigenvalue problem, and the primary task is to evaluate the eigenvalue relation

$$g(\alpha, \beta, \omega, R) = 0 \qquad (19)$$

for one parameter in terms of the others.

3. Orr-Sommerfeld Equation

If (13) and (15) are combined to form $\alpha f + \beta h$, this combination can be eliminated by (16), and, after differentiation, π' can be eliminated by (14) to give

$$\phi^{iv} - 2(\alpha^2 + \beta^2) \, \phi'' + (\alpha^2 + \beta^2)^2 \, \phi$$

$$= iR\left\{(\alpha U + \beta W - \omega) \, [\, \phi'' - (\alpha^2 + \beta^2) \, \phi]\right.$$

$$\left. - (\alpha U'' + \beta W'') \, \phi\right\}. \qquad (20)$$

When $W = 0$, this equation reduces to the equation obtained by Squire,[34] and when in addition $\beta = 0$, to

$$\phi^{iv} - 2\alpha^2\phi'' + \alpha^4\phi$$

$$= iR \, [\, (\alpha U - \omega)(\phi'' - \alpha^2\phi) - \alpha U'' \, \phi] \, . \qquad (21)$$

This is the Orr-Sommerfeld equation and is the basis for most of the work done in incompressible stability theory.

The Orr-Sommerfeld equation is a fourth-order equation and applies to a two-dimensional boundary layer. However, we can observe that (20), which is

the equation for a three-dimensional disturbance in a three-dimensional boundary layer, is also a fourth-order equation. This fact can be exploited to relate more general cases to (21). We will illustrate this possibility with Squire's equation. With $W = 0$, the transformation

$$\alpha^2 + \beta^2 = \tilde{\alpha}^2 \,, \quad R\alpha = \tilde{R}\tilde{\alpha}, \quad \omega\tilde{\alpha} = \tilde{\omega}\alpha \tag{22}$$

reduces (20) to

$$\phi^{iv} - 2\tilde{\alpha}^2\phi'' + \tilde{\alpha}^4\phi = i\tilde{R} \left[(\tilde{\alpha}U-\tilde{\omega})(\phi''-\tilde{\alpha}^2\phi) \right.$$

$$\left. - \tilde{\alpha}U''\phi \right], \tag{23}$$

which is identical to (21), but in the transformed variables. Since U is unchanged, it is evident that if α and β are real, a three-dimensional stability problem at Reynolds number R has been reduced to a two-dimensional problem at the lower Reynolds number $\tilde{R}$. This is the celebrated Squire theorem which states that in a two-dimensional boundary layer with real wave numbers, instability appears first for a two-dimensional disturbance. Further-more, if $\tilde{\omega} = \tilde{\omega}(\tilde{\alpha}, \tilde{R})$ has been determined for a given $U(y)$, then $\omega = \omega(\alpha, \beta, R)$ is immediately known from (22).

However, if α and β are complex or the boundary layer is three dimensional, the utility of the above transformation is lost. In the first instance, $\tilde{R}$ is complex, and in the second the boundary-layer profile is not invariant under the transformation. In both of these cases, there is little point in proceeding beyond (20). The important conclusion is that in stability problems governed by

(7)-(10), the determination of the eigenvalues only requires the solution of a fourth-order equation.

4. System of First-Order Equations

Since there are numerous stability problems that cannot be reduced to a fourth-order system, a more flexible approach is to abandon the Orr-Sommerfeld equation altogether and work in terms of a system of first-order equations. This approach can be illustrated with (7)-(10) although it doesn't reveal its full advantage until the eigenvalue problem is of higher than fourth order.

Let

$$\alpha f + \beta h = \tilde{\alpha}\tilde{f}, \quad \alpha h - \beta f = \tilde{\alpha}\tilde{h} . \tag{24}$$

By adding and subtracting (7) and (9), the following replacement equations can be formed for these two linear combinations:

$$i(\alpha U + \beta W - \omega) \, \tilde{\alpha}\tilde{f} + (\alpha U' + \beta W') \, \phi$$

$$= - i\pi(\alpha^2 + \beta^2) + \frac{1}{R} [\tilde{\alpha}\tilde{f}'' - (\alpha^2 + \beta^2) \, \tilde{\alpha}\tilde{f}] , \tag{25}$$

$$i(\alpha U + \beta W - \omega) \, \tilde{\alpha}\tilde{h} + (\alpha W' - \beta U') \, \phi$$

$$= \frac{1}{R} [\tilde{\alpha}\tilde{h} - (\alpha^2 + \beta^2) \, \tilde{\alpha}\tilde{h}] . \tag{26}$$

With,

$$Z_1 = \tilde{\alpha}\tilde{f}, \quad Z_2 = \tilde{\alpha}\tilde{f}', \quad Z_3 = \phi, \quad Z_4 = \pi,$$

$$Z_5 = \tilde{\alpha}\tilde{h}, \quad Z_6 = \tilde{\alpha}\tilde{h}', \tag{27}$$

the four equations (25), (8), (26), (10) can be written

$$z_1' = z_2 , \tag{28}$$

$$z_2' = [\alpha^2 + \beta^2 + iR(\alpha U + \beta W - \omega)] \, z_1$$

$$+ (\alpha U' + \beta W') \, R \, z_3 + i(\alpha^2 + \beta^2) \, R \, z_4, \tag{29}$$

$$z_3' = - i \, z_1, \tag{30}$$

$$z_4' = - \frac{1}{R} z_1' - [i(\alpha U + \beta W - \omega) + \frac{\alpha^2 + \beta^2}{R}] \, z_3, \tag{31}$$

$$z_5' = z_6, \tag{32}$$

$$z_6' = (\alpha W' - \beta U') \, R \, z_3$$

$$+ [\alpha^2 + \beta^2 + iR(\alpha U + \beta W - \omega)] \, z_5 . \tag{33}$$

The fact that the first four of these equations do not contain z_5 or z_6 confirms that the eigenvalues can be obtained from a fourth-order system even though we are really dealing here with a sixth-order system. It is only the determination of all of the eigenfunctions that requires the solution of the full sixth-order system. This formulation is applicable when α and β are complex and to three-dimensional boundary layers. The quantity $\tilde{\alpha}$ has been introduced only to connect with other formulations, but has not been assigned a meaning. When α and β are real, $\tilde{\alpha}$ is obviously the wave number in the direction of wave propagation.

In the freestream, (28)-(33) have constant coefficients and thus solutions of the form

$$z^{(i)}(y) = A^{(i)} \exp(\lambda_i y) \; . \tag{34}$$

The characteristic values occur in pairs, and are easily determined to be

$$\lambda_{1,2} = \mp (\alpha^2 + \beta^2)^{1/2} \; , \tag{35}$$

$$\lambda_{3,4} = \mp [\alpha^2 + \beta^2 + iR (\alpha U_1 + \beta W_1 - \omega)]^{1/2} \; , \tag{36}$$

$$\lambda_{5,6} = \lambda_{3,4} \; , \tag{37}$$

where U_1 and W_1 are the freestream values of $U(y)$ and $W(y)$. Only the upper sign satisfies the boundary conditions at $y \to \infty$. The characteristic functions for λ_1 are

$$A^{(1)}_1 = - i(\alpha^2 + \beta^2)^{1/2} \; , \tag{38}$$

$$A^{(1)}_2 = i(\alpha^2 + \beta^2) \; , \tag{39}$$

$$A^{(1)}_3 = 1 \; , \tag{40}$$

$$A^{(1)}_4 = i(\alpha U_1 + \beta W_1 - \omega)/(\alpha^2 + \beta^2)^{1/2} \; , \tag{41}$$

$$A^{(1)}_5 = 0 \; , \quad A^{(1)}_6 = 0 \; . \tag{42}$$

For real α, β and ω this solution is the linearized potential flow over a wavy wall moving in the direction of the wave number vector with velocity $\omega/(\alpha^2 + \beta^2)^{1/2}$. It can be called the inviscid solution, although this interpretation is valid only in the freestream. The characteristic functions for λ_3 are

$$A_1^{(3)} = - i[\alpha^2 + \beta^2 + iR(\alpha U_1 + \beta W_1 - \omega)]^{1/2} \, , \tag{43}$$

$$A_2^{(3)} = [\alpha^2 + \beta^2 + iR(\alpha U_1 + \beta W_1 - \omega)] \, , \tag{44}$$

$$A_3^{(3)} = 1 \tag{45}$$

$$A_4^{(3)} = 0, \quad A_5^{(3)} = 0, \quad A_6^{(3)} = 0 \, . \tag{46}$$

This solution represents a viscous wave and can be called the viscous solution. The third solution is another viscous solution, and is

$$A_1^{(5)} = 0, \quad A_2^{(5)} = 0, \quad A_3^{(5)} = 0, \quad A_4^{(5)} = 0 \, , \tag{47}$$

$$A_5^{(5)} = 1 \, , \tag{48}$$

$$A_6^{(5)} = - [\alpha^2 + \beta^2 + iR(\alpha U_1 + \beta W_1 - \omega)]^{1/2} \tag{49}$$

These three linearly independent solutions are the key to the numerical method of obtaining eigenvalues as they provide the initial conditions of the numerical integration.

B. Temporal and Spatial Theory

If α, β and ω are all real, the disturbance propagates through the parallel mean flow with constant rms amplitude. If α and β are real, and ω is complex, the amplitude will change with time; if α and β are complex, and ω is real, the amplitude will change with x and z. The former case is referred to as the temporal amplification theory, the latter as the spatial amplification theory. If all three quantities are complex, the disturbance will grow in both space and time. The original, and for many years the only, form of the theory was the temporal theory. However, in a steady mean flow the amplitude at a fixed point is independent of time and it changes only with distance. The spatial theory gives this amplitude change in a more direct manner than does the temporal theory.

1. Temporal Amplification Theory

With $\omega = \omega_r + i\omega_i$ and α and β real, the disturbance can be written

$$q'(x,y,z,t) = q(y) \exp (\omega_i t) \exp [i(\alpha x + \beta z - \omega_r t)] . \qquad (50)$$

The magnitude of the wave number vector is

$$\tilde{\alpha} = (\alpha^2 + \beta^2)^{1/2} , \qquad (51)$$

and the angle between the direction of $\tilde{\alpha}$ and the x axis is

$$\psi = \tan^{-1} (\beta/\alpha) \qquad (52)$$

The phase velocity, or the velocity with which the crests move normal to themselves, is

$$c_{ph} = \omega_r/\tilde{\alpha} \quad . \tag{53}$$

If A represents the magnitude of q' at some particular y, say the y for which $|q'|$ is a maximum, then it follows from (50) that

$$(1/A)(dA/dt) = \omega_i \quad . \tag{54}$$

We can identify ω_i as the temporal amplification rate. Obviously A could have been chosen at any y, and (54) would be the same. It is this property that enables us to talk about the "amplitude" of an instability wave in the same manner as the amplitude of a water wave even though this amplitude is a function of y. We may distinguish three possible cases:

$$
\begin{array}{ll}
\omega_i < 0 & \text{damped disturbances,} \\
\omega_i = 0 & \text{neutral disturbances,} \\
\omega_i > 0 & \text{amplified disturbances.}
\end{array}
\tag{55}
$$

The complex frequency may be written

$$\omega = \alpha c = \alpha(c_r + i\, c_i) \quad . \tag{56}$$

The real part of c is equal to the phase velocity c_{ph}, and αc_i is the temporal amplification rate. The quantity c appears frequently in the literature of stability theory. However, it cannot be used in the spatial theory, and since wave theory usually employs $\tilde{\alpha}$ and ω, with the phase velocity being introduced as needed, we will adopt the same procedure.

2. Spatial Amplification Theory

In the spatial theory, ω is real and the wave numbers in the x and z directions are complex. With

$$\alpha = \alpha_r + i\,\alpha_i, \qquad \beta = \beta_r + i\,\beta_i \quad , \tag{57}$$

we can write the disturbance in the form

$$q'(x,y,z,t) = q(y)\,\exp\left[-(\alpha_i x + \beta_i z)\right]\,\exp\left[i(\alpha_r x + \beta_r z - \omega t)\right] \quad . \tag{58}$$

By analogy with the temporal theory, we may define a real wave number by

$$\tilde{\alpha}_r = (\alpha_r^2 + \beta_r^2)^{1/2} \quad . \tag{59}$$

The angle between the direction of $\tilde{\alpha}_r$ and the x axis is given by

$$\psi = \tan^{-1}(\beta_r/\alpha_r) \quad , \tag{60}$$

and the phase velocity is

$$c_{ph} = \omega/\tilde{\alpha}_r \tag{61}$$

At this point, it is tempting to form a complex wave number $\tilde{\alpha}$ by (51) with the real part given by (59) and the imaginary part by a similar equation in terms of α_i and β_i. However, this procedure is valid only when

$$\beta_i/\alpha_i = \beta_r/\alpha_r \quad , \tag{62}$$

and it is not possible to make this assumption and have the spatial theory produce reasonable results. Instead it is necessary to separate the wave amplification from its orientation and introduce the new quantity

$$\bar{\alpha}_i = (\alpha_i^2 + \beta_i^2)^{1/2} \quad , \tag{63}$$

which makes an angle

$$\bar{\psi} = \tan^{-1} (\beta_i/\alpha_i) \tag{64}$$

with the x axis. If $\tilde{x}$ is the coordinate in the direction of $\bar{\alpha}_r$ and $\bar{x}$ is the coordinate in the direction of $\bar{\alpha}_i$, we can rewrite (58) as

$$q'(x,y,z,t) = q(y) \exp (- \bar{\alpha}_i \bar{x}) \exp [i(\tilde{\alpha}_r \tilde{x} - \omega t)] \quad . \tag{65}$$

It follows that the spatial amplification rate is

$$(1/A) (dA/d\bar{x}) = - \bar{\alpha}_i \quad . \tag{66}$$

To be more precise, (66) gives the maximum spatial amplification rate for the particular choice of $\bar{\psi}$; there are lesser amplification rates in other directions, and of course $\bar{\alpha}_i$ is itself a function of $\bar{\psi}$. We see that for three-dimensional waves the spatial theory has a difficulty not present in the temporal theory: in addition to the wave orientation angle ψ, the maximum amplification direction $\bar{\psi}$ must be specified before any calculations can be made.

•

The three cases which correspond to (55) in the temporal theory are:

$$\bar{\alpha}_1 > 0 \qquad \text{damped disturbances,}$$

$$\bar{\alpha}_1 = 0 \qquad \text{neutral disturbances,} \qquad (67)$$

$$\bar{\alpha}_1 < 0 \qquad \text{amplified disturbances.}$$

3. Relation Between Temporal and Spatial Theories

We now have a temporal theory in which the computation of the eigen-values is straightforward, but which does not yield a spatial amplification rate, and a spatial theory which yields a spatial amplification rate, but only after the unknown angle $\bar{\psi}$ has been specified. The problem of choosing $\bar{\psi}$ is avoided only in the special case of a two-dimensional disturbance in a two-dimensional boundary layer where both ψ and $\bar{\psi}$ are zero. The resolution of both of these dilemmas is provided by introducing the powerful concept of group velocity.

A laminar boundary layer is a dispersive medium for the propagation of instability waves. That is, different frequencies propagate with different phase velocities, so that the individual harmonic components in a group of waves at one time will be dispersed (displaced) from each other at some later time. An overall quantity, such as the energy density or amplitude, does not propagate with the phase velocity, but with the group velocity. Furthermore, the group velocity can be considered a property of the individual waves, and to follow an individual frequency we use the group velocity of that frequency. Consequently, an observer travelling with the group velocity of a particular frequency will always see that frequency and its associated amplitude. These concepts were originally developed for fully dispersed wave trains in a homo-

geneous medium with no dissipation (real α, β, ω). However, if the inhomo-geneity of the medium and the wave attenuation or amplification are both "small" over a wavelength, then the concepts still apply. The meaning of "small" can be made more precise by a multiple-scale perturbation analysis. These conditions appear to be satisfied for Tollmien-Schlichting waves in moderately unstable boundary layers. In addition, an initial arbitrary waveform quickly becomes the dispersed wave train of the theory because, as shown by Mack[35] for the temporal theory and by Corner, Houston and Ross[36] for the spatial theory, all other modes except the fundamental (Tollmien-Schlichting) mode are heavily damped. The basic ideas of linear dispersive wave theory for conservative systems are thoroughly discussed by Whitham.[37] An application to the non-conservative boundary layer has been made by Landahl[38] (but see also the criticism by Stewartson[39]).

The dispersion relation is

$$\omega = \omega(\alpha, \beta, x, z) \quad , \tag{68}$$

and the components of the (vector) group velocity in the x and z directions are obtained by differentiating (68) with respect to α and β. When α, β and ω are real,

$$c_g = \left(\frac{\partial \omega}{\partial \alpha} , \frac{\partial \omega}{\partial \beta} \right) \quad . \tag{69}$$

This same expression can be used in the temporal theory with ω replaced by ω_r, and in the spatial theory with α_r and β_r for α and β. The imaginary part of the group velocity is neglected (and is zero at the point of maximum amplification rate).

From what has already been said, it is clear that the temporal and spatial amplification rates are related by the group velocity. That is, from the parallel-flow temporal viewpoint we can form a spatial amplification rate by following the wave with the group velocity (now independent of x and z). The time derivative is thus transformed into a space derivative by

$$\frac{d}{dt} = c_g \frac{d}{d\bar{x}} \quad .$$
(70)

where $\bar{x}$ must be in the direction of c_g. Consequently,

$$\bar{\alpha}_i = - \frac{\omega_i}{|c_g|^2} c_g \quad ,$$
(71)

and the direction of $\bar{\alpha}_i$ can be written

$$\bar{\psi} = \tan^{-1} \left[(\partial\omega_r/\partial\beta)/(\partial\omega_r/\partial\alpha) \right] \quad .$$
(72)

The group velocity referred to here is the group velocity of the temporal theory.

The problem of converting a temporal to a spatial amplification rate was first encountered by Schlichting[4], who used the two-dimensional versions of (71) and (69) without comment. The same relation was also used later by Lees[40], but the first mathematical derivation was given by Gaster[41] for the two-dimensional case. The derivation of Gaster's relation is quite simple and can easily be generalized to three dimensions. The derivation starts from the fact that the complex frequency ω is an analytic function of the complex variables α and β at a fixed x an'   Therefore, the Cauchy-Riemann equations

The header 77-15 at top.

$$\frac{\partial \omega_r}{\partial \alpha_r} = \frac{\partial \omega_i}{\partial \alpha_i} \quad , \quad \frac{\partial \omega_r}{\partial \alpha_i} = -\frac{\partial \omega_i}{\partial \alpha_r} \quad ,$$

$$\frac{\partial \omega_r}{\partial \beta_r} = \frac{\partial \omega_i}{\partial \beta_i} \quad , \quad \frac{\partial \omega_r}{\partial \beta_i} = -\frac{\partial \omega_i}{\partial \beta_r} \quad , \tag{73}$$

can be applied. In the two-dimensional case, the left-hand side of the first of these equations is the group velocity. The derivative on the right-hand side can be approximated by noting that ω_i decreases from its temporal value to zero in the spatial theory as α_i goes from zero to its value in the spatial theory. If the amplification rate is small, these variations can be considered linear, and

$$\frac{\partial \omega_r}{\partial \alpha_r} = c_g \cong -\frac{\omega_i}{\alpha_i} \quad . \tag{74}$$

We see that (74) is the same as the two-dimensional form of (71) with the important difference that the relation is revealed to be only an approximation valid for small α_i. In the three-dimensional case, if $\bar{\psi}$ is specified arbitarily and the x axis rotated to lie in the $\bar{\psi}$ direction, (74) will still apply with α_i replaced by $\bar{\alpha}_i$ and c_g by the component of the group velocity in the $\bar{\psi}$ direction. Consequently, when $\bar{\psi}$ is chosen in the direction of the group velocity, (71) immediately follows, but again as an approximation rather than as an exact expression.

C. Numerical Procedures

1. Types of Methods

Since the early 1960's, the asymptotic theory developed by Tollmien[3] and Lin[4] has been largely superseded as a means of producing numerical results in favor of direct solutions of the governing differential equations on a

digital computer. The numerical methods employed fall roughly into three categories: (i) finite difference methods, first employed by Thomas[42] in his pioneering numerical work of 1953; (2) shooting methods, first employed by Brown[11] (a successful low Reynolds number program was operating as early as 1954); and (3) spectral methods, first used by Gallagher and Mercer[43] with Chandrasekhar and Reid functions, and later improved by Orszag[44] with the use of Chebyshev polynomials. All of these methods have advantages and disadvantages which show up in specialized situations, but all are probably equally able to do the routine eigenvalue computations required in transition prediction calculations. However, it is the shooting methods that have mainly been applied to this problem and will be described here.

After Brown's initial work, programs were developed by Mack,[45] Landahl and Kaplan,[16] Radbill and Van Driest,[46] Lee and Reynolds,[47] Wazzan, Okamura and Smith,[17] and Davey,[48] among others. Most of these programs solve only the Orr-Sommerfeld equation; exceptions are the compressible program of Brown,[14] and the program of Mack[45] which was also originally developed for compressible flow and only later extended to incompressible flow. All of the programs except Brown's have the common feature that the numerical integration proceeds from the freestream to the wall.

The early applications of shooting methods suffered from the problem of parasitic error growth. This growth arises because of the presence of a rapidly growing solution (the local "viscous" solution) which any numerical roundoff error will follow. The rapidly growing error eventually completely contaminates the less rapidly growing solution. The essential advance in coping with this problem, which had previously limited numerical solutions to moderate Reynolds number, was made by Kaplan.[49] The Kaplan method "purifies"

the contaminated solution by filtering out the parasitic error whenever it becomes large enough to destroy linear independence.

2. Gram-Schmidt Orthonormalization

An alternative method, first employed by Bellman and Kalaba[50] and applied to the stability problem by Radbill and Van Driest[46] and Wazzan, Okamura and Smith,[17] is that of Gram-Schmidt orthonormalization. This method has the advantage that it is easier to generalize to higher-order systems than is the Kaplan filtering technique. However, the geometrical argument often adduced in its support that this procedure preserves linear independence by keeping the solution vectors orthogonal cannot be correct because the solution vector space does not have a metric. Instead, the method works on exactly the same basis as Kaplan filtering: the "small" solution is replaced by a linear combination of the "small" and "large" solutions which is itself constrained to be "small."

For the simplest case of a two-dimensional wave in a two-dimensional boundary layer, there are two solutions, $z^{(1)}$ and $z^{(3)}$, each consisting of four components. In the freestream, $z^{(1)}$ is the inviscid and $z^{(3)}$ the viscous solution. Although this identification is lost in the boundary layer, $z^{(3)}$ continues to grow more rapidly with decreasing y than does $z^{(1)}$. The parasitic error will follow $z^{(3)}$, and when the difference in the magnitudes of $z^{(3)}$ and $z^{(1)}$ exceeds the computer word length, $z^{(1)}$ will no longer be independent of $z^{(3)}$. Well before this occurs, the Gram-Schmidt orthonormalization algorithm is applied. The "large" solution $z^{(1)}$ is normalized component by component to give the new solution

$$s^{(3)} = z^{(3)}/\{z^{(3)*} z^{(3)}\}^{1/2} , \tag{75}$$

where the asterisk refers to a complex conjugate and {} to a scalar product. The scalar product of $Z^{(1)}$ and $S^{(3)}$ is used to form the vector

$$S^{(1)} = [Z^{(1)} - \{S^{(3)*} Z^{(1)}\} S^{(3)}]/\{\bar{S}^{(1)*} \bar{S}^{(1)}\}^{1/2} \tag{76}$$

to replace $Z^{(1)}$, where $\bar{S}$ refers to the quantity in the preceding square brackets.

The numerical integration continues with $S^{(1)}$ and $S^{(3)}$ in place of $Z^{(1)}$ and $Z^{(3)}$, and when in turn $|S^{(3)}|$ exceeds the set criterion of, say 10^5 with single precision arithmetic and a 36 bit computer word, the orthonormalization is repeated. With homogeneous boundary conditions at the wall, it makes no difference in the determination of the eigenvalues whether the Z's or S's are used. A linear combination of the two solutions satisfies the $f(0) = 0$ boundary condition, but the $\phi(0) = 0$ boundary condition will in general not be satisfied unless α, β and ω satisfy an eigenvalue relation.

3. Newton-Raphson Search Procedure

The Newton-Raphson method has been found to be satisfactory for obtaining the eigenvalues. In the spatial theory with ω and β fixed, the guess value of α_r is perturbed by a small amount ($\Delta = 0.001 \, \alpha_r$) and the integration repeated. Because $\phi(0)$, the third component of the linear combination of the two independent solutions $Z^{(1)}$ and $Z^{(2)}$ (or $S^{(1)}$ and $S^{(2)}$) which satisfies $f(0) = 0$, is an analytic function of the complex variable α, even after orthonormalization, the Cauchy-Riemann equations

$$\frac{\partial \phi_i(0)}{\partial \alpha_i} = \frac{\partial \phi_r(0)}{\partial \alpha_r} \quad ,$$

$$\frac{\partial \phi_r(0)}{\partial \alpha_i} = - \frac{\partial \phi_i(0)}{\partial \alpha_r} \quad , \tag{77}$$

can be applied to eliminate the need for a second integration with α_i perturbed.

The corrections $\delta\alpha_r$ and $\delta\alpha_i$ to the initial guesses α_r and α_i are obtained from the residual $\phi(0)$ and the numerical (linear) approximations to the partial derivatives by the equations

$$\frac{\partial\phi_r(0)}{\partial\alpha_r}\,\delta\alpha_r + \frac{\partial\phi_r(0)}{\partial\alpha_i}\,\delta\alpha_i = -\,\phi_r(0) \quad ,$$

$$\frac{\partial\phi_i(0)}{\partial\alpha_r}\,\delta\alpha_r + \frac{\partial\phi_i(0)}{\partial\alpha_i}\,\delta\alpha_i = -\,\phi_i(0) \quad . \tag{78}$$

The corrected α_r and α_i are used to start a new iteration, and the process continued until $\delta\alpha_r$ and $\delta\alpha_i$ have been reduced below a preset criterion.

4. A Numerical Example

As an example we will consider that the Reynolds number and frequency are specified for the flat-plate boundary layer, and we wish to determine both the complex wave number of the spatial theory and the wave number and amplification rate of the temporal theory. It is convenient to define the length scale as

$$L^* = (\nu^* x^*/U_1^*)^{1/2} \quad . \tag{79}$$

With this choice, the Reynolds number is

$$R = U_1^* L^*/\nu^* = (U_1^* x^*/\nu^*)^{1/2} = Re^{1/2} \quad . \tag{80}$$

The Reynolds numbers and wave numbers based on the displacement, momentum and boundary-layer thicknesses are obtained by multiplying R and α based on L^* by

-25-

the appropriate dimensionless thickness. For the flat-plate boundary layer, these factors are, in the above order, 1.7208, 0.66411 and 6.0114 (u/U_1 = 0.999). The usual form of the dimensionless frequency is

$$F = \omega^* \nu^* / U_1^{*2} = \omega/R \ . \tag{81}$$

For the example, we choose

$$R = 1000, \quad F = 0.3 \times 10^{-4},$$

and for the initial guess of the complex α in the spatial theory,

$$\alpha_r = 0.12 \ , \quad \alpha_i = -5.0 \ ;$$

and for the temporal theory,

$$\alpha_r = 0.12 \ , \quad \omega_i = 10.0 \ .$$

The initial conditions of the two independent solutions are evaluated from the formulas of Section II-A.4, and the numerical integration started at $y_1 = y^*/L^* = 8.0$. Each solution is integrated to the wall (at $y = 0$) by means of a fourth-order, fixed step size, Runge-Kutta integration. Other integration methods are also satisfactory, but this simple method has been found to be trustworthy in a wide variety of problems, particularly in the difficult problem of determining the eigenvalue spectrum.[35] Variable step-size integrators are not recommended.

The operation of the eigenvalue search procedure is shown in Table I. The search is continued until $\delta|\alpha|/|\alpha|$ is reduced below a preset criterion (0.005 is usually adequate for three-place accuracy) in the spatial theory, and $\delta\alpha/\alpha$ and $\delta|\omega_i|/|\omega_i|$ separately satisfy the criterion in the temporal theory. Since ω_r is held constant in the temporal theory, two perturbation integrations are required per iteration instead of one as in the spatial theory. Two iterations are usually sufficient to achieve convergence in a large scale computation where previously calculated eigenv. les can be used to make good initial guesses. Poor initial guesses were deliberately chosen in the examples.

Once a single eigenvalue has been found for a given boundary layer, all others can be readily obtained. Automatic procedures can be included in the program to produce all of the unstable eigenvalues of a given frequency or wave number mesh up to some specified large Reynolds number in a single computer run of a few minutes for a two-dimensional boundary layer. The problem of obtaining the initial eigenvalue can prove troublesome. If the boundary layer under investigation is not far removed from one for which the eigenvalues are known, it is always possible to make a close enough guess for the Newton-Raphson procedure to converge. If not, it is necessary to perform individual integrations in the complex α plane (spatial) or ω plane (temporal). Then the contour line method of Mack,[35] or the more elaborate methods of Antar[51] and Jordinson and Gaster,[52] can be used to locate the initial eigenvalue.

D. Some Numerical Results

1. Amplification Properties of Falkner-Skan Profiles

For a two-dimensional incompressible boundary layer on an impermeable surface of zero curvature and with no body force or surface heating, the only flow parameter left is the pressure gradient. The effect on the amplification

properties of systematic changes in the pressure gradient can best be demonstrated with the Falkner-Skan family of similar velocity profiles. The single parameter of a Falkner-Skan boundary layer is the dimensionless pressure gradient

$$m = - \frac{x^*}{\rho^* U_1^{*2}} \frac{dp^*}{dx^*} = \frac{x^*}{U_1^*} \frac{dU_1^*}{dx^*} \ . \tag{82}$$

It is usual to replace m by

$$\beta = 2m/(m + 1) \tag{83}$$

(not to be confused with the lateral wave number). The values of β range from 1.0 for the two-dimensional stagnation point boundary layer, through $\beta = 0$ for the flat plate, to $\beta = 0.1988377$ for the separation profile. More negative values of β represent reverse-flow profiles.

Two theoretical principles are useful in interpreting the numerical results. The first comes from the viscous asymptotic theory, and states that increasing the negative curvature of the velocity profile near the wall increases the stability. The second comes from the inviscid theory of Rayleigh and states that as the inflection point moves away from the wall, the profile becomes more unstable. We need only recall that as β increases from zero, the first effect occurs; as it decreases from zero, the second affect occurs.

Some properties of Falkner-Skan profiles are summarized in Table II, where are listed δ^*, θ and δ (the displacement, momentum and boundary-layer thicknesses)made dimensionless with respect to L^*; $H = \delta^*/\theta$, the shape factor; $U''(0)$ $(= - m)$, the curvature at the wall; y_s/δ, the location of the

inflection point; and c_s, the dimensionless velocity at the inflection point and equal to the phase speed of the neutral inviscid disturbance.

The temporal stability of Falkner-Skan profiles was computed in great detail by Pretsch[8] from the asymptotic theory (these results may also be found in Smith and Gamberoni[53]), and both the temporal and spatial stability from direct numerical solutions by Wazzan, Okamura and Smith.[17,18] For application to the transition problem, the quantity of primary interest is the integral of the spatial amplification rate for a constant frequency. With L^* still defined by (79), R by (80) and U_1^* by (82), it follows from (66) that

$$\ln\left(\frac{A}{A_o}\right) = -\frac{2}{m+1}\int_{R_o}^{R}\alpha_i\ dR\ , \tag{84}$$

where A_o is the amplitude at the initial Reynolds number R_o. It is convenient to take R_o as the lower-branch neutral stability point (initial point of instability for the frequency under consideration) in order to give a unique meaning to A/A_o. If the definition of the dimensionless frequency given by (81) is to be retained, then F is no longer constant for a constant dimensional frequency, but is given by

$$F(R) = \frac{\omega^* \nu^*}{U_1^{*2}(x^*)} = \frac{\omega^* \nu^*}{U_1^{*2}(x_o^*)}\left(\frac{R_o}{R}\right)^{4m/m+1}. \tag{85}$$

Thus the calculation starts at $R_o^2 = U_1^*(x_o^*)\ x_o^*/\nu^*$ with dimensionless frequency $F_o = \omega^* \nu^*/U_1^{*2}(x_o^*)$, and the integral (84) is evaluated using $\alpha_i(R)$ calculated with the F(R) from (85).

The length scale L^* is not the only possible choice with which to make α_i^* dimensionless. The inverse of the unit Reynolds number, ν^*/U_1^*, is often found in the literature.[17,18,49] With this choice,

$$\ln\left(\frac{A}{A_o}\right) = -\frac{1}{m+1} \int_{Re_o}^{Re} \frac{\alpha_i^* \nu^*}{U_1^*} \, d\,Re \quad , \tag{86}$$

where Re is the x-Reynolds number. This procedure is perfectly acceptable, but it has the disadvantage that $\alpha_i^* \nu^*/U_1^*$ ($= \alpha_i/R$) always goes to zero as Re $\to \infty$ even when the boundary layer is unstable to inviscid disturbances. On the contrary, the quantity α_i is based on a boundary-layer length scale, and so can also be used as the inviscid amplification rate. Comparisons are easy to make between the viscous and inviscid stability theories in terms of α_i. For example, with $\beta = -0.15$, the inviscid $(-\alpha_i)_{max}$ is 0.0199, and in the viscous theory $(-\alpha_i)_{max}$ already reaches the slightly higher value of 0.0202 at the low Reynolds number of R = 400.

For the transition-prediction calculations of Section IV, three quantities will be needed: (i) the envelope curve, $\ln (A/A_o)_{max}$ vs. R, formed by the individual $\ln (A/A_o)$ vs. R curves; (ii) the frequency, F_{max}, of the envelope curve; and (3) a bandwidth ΔF of the frequency response curves to be discussed below. The envelope curves for several values of β are shown in Figure 1. Both the strong stabilizing effect of a favorable pressure gradient, and the even stronger destabilizing effect of an adverse pressure gradient are clearly evident. The corresponding frequencies are shown in Figure 2. (The $\beta = -0.05$ curve is almost coincident with the $\beta = 0$ curve and so cannot be shown.) We see a clear distinction between

viscous and inflectional instability. Viscous instability is primarily a low frequency instability, particularly when the instability only develops at high Reynolds numbers. In contrast, inflectional instability is a high frequency instability. The ratio of the frequency which gives ln (A/A_o) = 9 for β = -0.15 to the corresponding frequency for β = 0.20 is 36.

The need for quantity (iii) is shown in Figure 3, where ln (A/A_o) for the flat-plate boundary layer is plotted against F for several Reynolds numbers. As R increases, the maximum amplitude ratio increases and the band-width of unstable frequencies decreases. This sharpening of the boundary-layer response must be taken into account in any transition prediction method that attempts to calculate the integrated (over frequency) amplitude in the boundary layer. A quantitative measure of this effect is provided by the bandwidth

$$\Delta F = F_{max} - F[\ln (A/A_o)_{max} - 1] \quad , \tag{87}$$

where the second term is the frequency at which A/A_o is $1/e$ of $(A/A_o)_{max}$ on the low frequency side of F_{max}. It is desirable to define ΔF this way rather than as a two-sided bandwidth because the practical requirements of a large scale eigenvalue calculation are such that A/A_o can always be obtained for frequencies smaller, not larger, than F_{max}. Figure 4 gives the ratio $\Delta F/F_{max}$ as a function of R for the same β as in the previous figures.

2. Comparison of Temporal and Spatial Amplification Rates

The requirement to know the direction of the group velocity before computing eigenvalues from the spatial theory for other than two-dimensional

waves in two-dimensional boundary layers makes it worthwhile to examine how accurate are the spatial amplification rates obtained from the temporal theory and Gaster's relation in this more restricted case. The group velocity of the temporal theory, as given by (69), can be computed by numerical differentiation along with the other stability properties provided ω_r is a smoothly varying function of the wave number.

Table III presents both ω_i and α_i for four α_r (three amplified, including the maximum, and one damped) at three different β and at Reynolds numbers with large amplification rates. The case $\beta = 0$ provides amplification rates typical of boundary layers with small favorable pressure gradients; $\beta = -0.10$ provides about the largest amplification rates that can be expected in practice; and the separation profile can be viewed as providing an upper limit for boundary-layer amplification rates, but not particularly representative of actual practice. (The maximum amplification rate of this profile occurs at $R \rightarrow \infty$ and is -0.0480, which is only 12% larger than the $R = 300$ value of -0.0424.)

From Table III we see that the Gaster relation is satisfied quite well at $\beta = 0$, and less well at the two other β's. At $\beta = 0$, the frequency and phase velocity from the two theories also agree closely. It can also be noted that the ratio $- \omega_i/\alpha_i$ is less than the group velocity at the maximum amplification rate for all three values of β. The maximum difference between c_g and $-\omega_i/\alpha_i$ for amplified disturbances occurs at the maximum amplification rate, and is 1.6% for $\beta = 0$, 2.8% for $\beta = -0.10$, and 5.7% for the separation profile. In the latter case, there are also important differences in ω_r and c_{ph} between the two theories at both low and high wave numbers. The conclusion can be drawn from Table III that the temporal theory and Gaster's relation

of'er a satisfactory method of obtaining spatial amplification rates for zero and favorable pressure gradients, but that this approach becomes increasingly more unreliable as the adverse pressure gradient increases.

3. Group Velocity Direction for Oblique Waves

The importance of the choice of the direction of maximum amplification in the spatial theory can be readily demonstrated by means of oblique waves in the flat-plate boundary layer. Table IV gives results for the two-dimensional wave of dimensionless frequency $F = 0.3 \times 10^{-4}$ at $R = 1600$, and for three oblique waves with $\psi = 45^{\circ}$, 60° and 75°. The Reynolds numbers and F for these waves were chosen so that in the ψ direction the Reynolds number ($\check{R} = R \cos \psi$) and dimensionless frequency ($\check{F} = F/\cos^2 \psi$) are the same as for the two-dimensional wave. According to (22), the Squire transformation, the spatial amplification rate in the x-direction is

$$\alpha_i = \tilde{\alpha}_i \cos \psi \quad ,$$

where $\tilde{\alpha}_i$ is the spatial amplification rate of the two-dimensional wave with $F = 0.30 \times 10^{-4}$ at $R = 1600$. Since $\tilde{\alpha}_i = -3.82 \times 10^{-3}$ from Table IV, the other three values should be -2.70, -1.91, and -0.989 for $\psi = 45^{\circ}$, 60°, 75° respectively. We can see that, as already stated in Section II-A.2, this relation is true only when $\bar{\psi} = \psi$. For $\bar{\psi} < \psi$, α_i is larger than these values by amounts ranging up to 39%. Consequently, it is not ermissible to use $\bar{\psi} = \psi$ in order to preserve the real form of the Squire transformation.

The correct $\bar{\psi}$ is the direction of the group velocity. Figure 5 shows how this direction, now identified as $\dot{\psi}$ and computed from the temporal theory, varies with ψ for two fixed values of $\tilde{\alpha}$ at $R = 1600$. The important

conclusion to be drawn from Figure 5 is that regardless of the orientation of
the constant phase lines (the crests), the group lines, which give the
direction of energy propagation, remain concentrated near the freestream
direction. Furthermore, the 10° entry of Table IV shows that α_i is nearly
the same as with $\bar{\psi} = 0$. Thus, for oblique waves in a two-dimensional boundary
layer, it is a permissible approximation to use the spatial theory with $\bar{\psi} = 0^{\circ}$.
However, it is still necessary to use either the complex form of the Squire
transformation or the formulation given in Section II-A.4 to compute the
eigenvalues.

III. STABILITY EXPERIMENTS

A. Schubauer-Skramstad Experiment

The linear stability theory long went unappreciated except by its
founders because of the lack of any convincing experimental confirmation.
This needed confirmation was brilliantly supplied by the now classic experi-
ment of Schubauer and Skramstad[5] which was carried out at the National
Bureau of Standards in the early 1940's, but not published because of war-
time restrictions until 1948. This experiment owed its success both to the
ingenuity of the experimenters and to the development for the first time of a
wind tunnel with a really low turbulence level (about 0.03% in the working
section). When, with this low turbulence level, the signal of a hot-wire
anemometer placed in the boundary layer of a flat plate was displayed on an
oscilloscope screen, modulated sinusoidal wave trains with almost no random
character were clearly seen. Schubauer and Skramstad demonstrated conclusively
that these were true boundary-layer oscillations, and that they were the
cause, and not the effect, of transition.

In order to make a more quantitative connection with the theory of Tollmien and Schlichting, they used a vibrating ribbon in order to produce disturbances of a fixed frequency with a controlled initial amplitude. The hot wire then measured the wave length, phase velocity, and amplitude of the artificially produced waves as a function of Reynolds number. Numerous comparisons were made with the theory which were on the whole satisfactory, although the asymptotic theory at that time did not yield very accurate numerical results. However, it is well to emphasize that the virtue of this experiment did not lie in an exact quantitative correspondence with theory, but rather in the systematic way that all essential features of the theory were shown to be correct, and in the way the oscillations were shown to be necessary precursors of transition.

The hot wire measures directly the rms disturbance amplitude as a function of downstream distance, and the amplification rates must be deduced from the slopes of such measurements. Although the interpretation of the measured amplitude has difficulties associated with non-parallel flow effects, it is still of considerable interest to compare the amplitude measurements with the quantity A of stability theory. The comparison is given in Figure 6. The experimental wave amplitudes (u' at a fixed distance from the wall) are all referred to the amplitude at x_o = 2 in. behind the ribbon which was located 4 ft. behind the leading edge of the plate with U_1 = 64 ft/sec. Therefore, the integration of α_i was also started at x_o (R_o = 1256), and A_o is the amplitude at x_o rather than at the neutral stability point. The experimental points in Figure 6 show conclusively that the frequency is the fundamental parameter that determines whether a wave will be amplified or damped, and the agreement with theory is satisfactory although far from exact.

This is a good place to bring out some importa· quantitative aspects of instability waves. The ratio of the wavelength to t... displacement thickness is

$$\frac{\lambda}{\delta^*} = \frac{2\pi}{\alpha_r} \left(\frac{x}{\delta^* Re^{1/2}} \right) \quad . \tag{88}$$

At R ≈ 1256 (the x_o of Figure 6), α_r = 0.128 for the frequency with the largest amplification rate (f = 120 hz, F = 0.311 x 10^{-4}). Hence λ = 28.5 δ^* (= 8.2 δ), and we see that unstable Tollmien-Schlichting waves are long compared to the boundary-layer thickness. This result from a theory that assumes parallel flow was one of the original criticisms made of the theory, ᵗnd also explains why a considerable effort has been made recently to develop non-parallel theories.[32,33,54] Another interesting point is ᵗʰᵉ rapidity with which the waves grow. The 120 hz wave increases in amplitude 2.5 times in 6 in. (= 88 δ^*, or 3.1 λ). From the definition of the amplification rate, the fractional change in amplitude per wavelength, with α_i and α_r assumed constant, is

$$\frac{\delta A}{A} = \frac{2\pi\alpha_i}{\alpha_r} \quad , \tag{89}$$

or about 33% for the 120 hz wave. Although this large growth only exists near the maximum amplification rate, it still raises problems concerning the application of kinematic wave concepts to instability waves.

B. Other Older Experiments

The next stability experiments were carried out by Liepmann.[55,56] These experiments were designed primarily to study the stability and

transition of boundary layers on concave surfaces, i.e. Görtler instability,
but measurements were also made on the convex side of the curved plate. Two
plates were used, with radii of curvature of 20 ft. and 2-1/2 ft., but only
the 20 ft. plate was used for the detailed measurements on the convex side.
The boundary-layer velocity profile was close to that of a flat plate, but
the neutral-stability curve was found to define an unstable region somewhat
larger than in the Schubauer-Skramstad experiment, perhaps reflecting a
slight average adverse pressure gradient. Transition measurements on the
convex sides of both plates showed no effect of curvature, but the imposition
of favorable and adverse pressure gradients on the 20 ft. plate did produce
an effect. The transition Reynolds number was increased for a favorable and
decreased for an adverse pressure gradient, and the percentage change was
greater for the favorable pre.. ̇f gradient. No stability measurements were
made with a pressure gradier⸱ indeed no theoretical stability results
on the effect of pressure gra..⸱r. ⸱ere available to Liepmann at the time of
the experiments.

The next experiment, by Bennett,[57] studied the influence of freestream
turbulence on the instability of the flat-plate boundary layer. A grid was
installed upstream of the test section to raise the turbulence level to
0.42%. The signal from a hot wire in the laminar boundary layer showed
fluctuations of a random nature resembling turbulence with little evidence of
Tollmien-Schlichting waves, an observation in accord with Dryden's[58] work
of 20 years previously. However, when the power spectrum of the fluctuations
was measured with a wave analyzer, a local peak was found to develop at
about the most unstable frequency of linear stability theory. This peak
grew with increasing downstream distance, and gradually disappeared after
transition started as the spectrum evolved into one typical of a turbulent

boundary layer. Measurements were made at too few x stations in the laminar region to determine the amplitude history of the peak, and consequently no conclusion is possible from this experiment on the crucial point of whether the linear disturbance growth is affected by the external turbulence level.

A flow visualization technique for instability waves using tellurium coated rods was developed by Wortmann[59] for use in a water boundary layer. When a voltage was applied to the rods, tellurium ions, which are black, were released and made the instability waves clearly visible. It was then possible to make quantitative measurements, and a neutral stability curve was determined that compared favorably with Schubauer and Skramstad's. Other flow visualization techniques that have been used are smoke,[60,61] dye[62] and hydrogen bubbles.[63] These methods all show the presence of Tollmien-Schlichting waves, but have been applied mainly to study the details of the transition process following linear amplification.

The hot-wire anemometer continued to be the primary tool of the NBS transition studies, which, following the work of Schubauer and Skramstad, also concentrated on the non-linear region. Schubauer and Klebanoff[64] studied the characteristics of the turbulent spot; Klebanoff and Tidstrom[65] and Klebanoff, Tidstrom and Sargent[66] the sequence of events from the end of the linear region to the first appearance of a turbulent spot. It was found that the initially two-dimensional Tollmien-Schlichting wave develops a spanwise periodicity in amplitude while it is still undergoing linear amplification. There appears to be a characteristic spanwise wavelength that has since been observed in other wind tunnels, but no convincing explanation has yet been given for the origin of this periodicity. The Knapp and Roache[61] smoke pictures clearly show that a similar three-dimensionality also develops in natural transition.

C. Three Recent Experiments

1. Ross, Barnes, Burns and Ross Experiment

What amounts to a repetition of that part of the Schubauer-Skramstad experiment which measured the instability of a flat-plate boundary layer was carried out by Ross, Barnes, Burns and Ross.[67] Their wind tunnel had the same turbulence level as the NBS tunnel, was of similar size, the flat plate was also mounted vertically, and a vibrating ribbon was used to produce the instability waves. The hot-wire measurements were compared with the detailed calculations of Jordinson,[68] and excellent agreement was obtained for the distribution of u' through the boundary layer. Quite good agreement was also obtained for the A/A_0 of three frequencies $(F \times 10^4 = 0.82, 1.10, 1.57)$. Particular attention was paid to the region of the minimum critical Reynolds number and the maximum unstable frequency. Measurements in this region are difficult because the boundary layer is both thin and rapidly growing. A neutral-stability curve was arrived at with $R_{cr} = 230$ and $F_p = 4 \times 10^{-4}$ compared to the theoretical values of $R_{cr} = 302$ and $F_p = 2.5 \times 10^4$. The differences between theory and experiment were attributed to non-parallel flow effects, a supposition since confirmed by the good agreement of the Saric-Nayfeh theory[33] with the above experimental results.

It must be pointed out that the frequencies that define the R_{cr} portion of the neutral-stability curve are not those that are important to transition in environments with small disturbances. For example, at the Schubauer-Skramstad transition Reynolds number of 2.8×10^6, we see from figure 2 that $F_{max} = 0.29 \times 10^{-4}$ compared to $F = 3.5 \times 10^{-4}$ at $R_{cr} = 250$ according to Saric and Nayfeh. The former frequency first becomes unstable at $R = 820$, where the non-parallel flow effects are less severe than at the minimum critical Reynolds number. The non-parallel flow effects will be

even further reduced in boundary layers with favorable pressure gradients where instability occurs at much higher Reynolds numbers than for the flat plate.

2. Klebanoff-Tidstrom Experiment

It is surprising that tne traditional low-speed stability theory has never been tested experimentally for other than the Blasius boundary layer studied by Schubauer and Skramstad. There have been boundary-layer stability experiments on the effects of rotation,[69] compressibility,[70] free convection,[71] and a heated wall in water,[72] but the accompanying theories represented extensions of the existing theory to new flow situations. There have been transition experiments on the technically important effects of pressure gradient and suction, but no stability experiments.

There is an important aspect of transition that also has received little attention, and that is the relation of a particular disturbance source to the transition process in a boundary layer. In other words, the precise mechanism by which, say, freestream turbulence, sound, and different types of roughness cause transition remains to be discovered. Only in the case of two-dimensional roughness has the mechanism been found thanks to a remarkable experiment by K. anoff and Tidstrom.[73] For circular roughness elements with a diameter of about $0.8 \, \delta^*$, these investigators determined that transition was moved forward from its normal location, not by a disturbance introduced into the boundary layer by the roughness, but by the increased amplification of an already existing instability wave in the pressure recovery zone behind the roughness. In a certain sense, we do have here an example of a stability experiment with a pressure gradient, but this very special flow is scarcely representative of pressure-gradient boundary layers.

Although the demonstration by Klebanoff and Tidstrom of the actual transition mechanism was complete in itself and did not rely on theoretical comparisons, they did compare their disturbance growth measurements with results obtained from Pretsch's charts.[8] Unseparated adverse pressure gradient Falkner-Skan profiles were fitted to the measured profiles on the basis of the shape factor H. The calculated and measured growths were in good agreement. However, there are three objections that can be raised to Klebanoff and Tidstrom's procedure: (i) the profiles in the initial part of the recovery zone are clearly separated; (ii) the Pretsch charts are not very accurate for adverse pressure gradients; and (iii) the group, and not the phase, velocity should have been used to transform temporal to spatial amplification rates.

When the computation is repeated with the correct spatial amplification rates for the fitted Falkner-Skan profiles, the results are not in agreement with the measurements. The obvious next step is to use the correct velocity profiles which were measured in great detail and with little scatter. Unfortunately, the separated-flow region, which has a strong influence on the instability, could not be measured because of its closeness to the wall. In any case, stability calculations based on experimental curve fits to profiles with an inflection point are not likely to be meaningful. The conclusion to be drawn is that although the Klebanoff-Tidstrom experiment firmly established that two-dimensional roughness influences transition by destabilizing the boundary layer, the amplification measurements cannot be used as a test of a particular form of the stability theory in a rapidly varying pressure-gradient flow.

3. Gaster-Grant Experiment

Another recent stability experiment of great interest was carried out by Gaster and Grant[74] in the same wind tunnel used in the Ross, Barnes, Burns and Ross experiment.[67] All of the other stability experiments with artificially produced disturbances have followed directly in the Schubauer-Skramstad tradition of dealing with a Tollmien-Schlichting wave of a single frequency. This approach was followed even where the traditional vibrating ribbon was replaced by a siren[70] or a glow-discharge device.[75] In the latter instance, oblique waves were also produced, but still only of a single frequency. Gaster and Grant used the completely different approach of transmitting an acoustic pulse from a loudspeaker through a small hole in their flat plate to produce a pulse disturbance in the boundary layer. This disturbance, after the rapid decay of all higher modes consists of Tollmien-Schlichting waves of all frequencies and orientations. This type of experiment, while not as suited to mapping out stability boundaries and making the other usual checks of stability theory as in a vibrating ribbon experiment, is in some respects closer to the transition problem. An external disturbance, such as freestream turbulence or sound, will also produce Tollmien-Schlichting waves of all frequencies and orientations, but in a random manner that makes the ensuing wave motion in the boundary layer difficult to sort out. The pulse experiment gives a controlled disturbance of this type which enables the details of a group of waves (a wave packet), rather than a single Fourier component, to be investigated.

In the experiment, the hot wire was placed at 15 spanwise stations at each of six downstream locations to record the passage of the wave packet. Although several theoretical treatments of the motion of a pulse in a shear layer have appeared,[76-79] these papers all made use of asymptotic

methods. In order to have more exact numerical results, the amplitude of
the wave packet was calculated from

$$A(x,z,t) \sim \int_0^\infty \int_0^\infty x^{-1/4} \exp\left\{ i\left[\int_{x_o}^x \alpha(x)\ dx + \beta z - \omega t \right]\right\} d\beta\ d\omega \ , \qquad (90)$$

where x_o is the location of the pulse; and the Fourier coefficient has been
set equal to unity. The factor $x^{-1/4}$ is intended to account for the
effect of the boundary-layer growth, and the integral of $\alpha(x)$ appears
for this same reason. The eigenvalues $\alpha(x)$ were obtained from the
spatial stability theory for all values of β and ω by use of the Squire
transformation and a complex Reynolds number. In order to evaluate the
double integral with sufficient accuracy to reproduce the wave packet,
10,000 eigenvalues were needed. The agreement that was achieved
between theory and experiment for about the first 2/3 of the distance
covered was impressive. After this, the experimental wave packet
distorted in a way not given by the theory, possibly due to non-linear
effects.

IV. TRANSITION PREDICTION

A. Nature of the Problem

A boundary layer has a specific displacement thickness and skin friction, but it does not have a specific transition Reynolds number. The observed transition Reynolds number depends on the presence of disturbances in the boundary layer, which in turn are related to various disturbance sources. If there were no disturbances, there would be no transition and the boundary layer would remain laminar. Consequently, it is futile to talk about transition without in some way bringing in the disturbances which cause it, and any transition criterion of an empirical nature can only be valid for a very specific disturbance environment.

Another point which must be settled before going deeper into the subject is to define the circumstances under which linear theory can be used to predict transition. Disturbances such as a large three-dimensional roughness element, or an air jet, cause transition to occur in the immediate vicinity of their location. However, in many other instances, the disturbances act in a more indirect manner. A moderate freestream turbulence level or acoustic intensity affects transition by producing Tollmien-Schlichting waves in the boundary layer which then amplify, distort, and finally culminate in the sudden appearance of a turbulent spot.[64] These instability waves can be described initially by linear theory, and if the initial disturbance amplitude is sufficiently small, the region of linear growth can be of significant extent. In this case, the exponential growth of a linear disturbance, and the absence of an extensive region of distorted laminar flow before the sudden breakdown to turbulence that is such a distinguishing feature of low-speed boundary-layer transition, makes it feasible to base a method of transition prediction directly on the linear theory itself.

B. Amplitude Density Methods

1. Liepmann's Method

The first application of linear theory to transition, by Schlichting,[4] has already been mentioned in Section I. A later method, developed by Schlichting for application to airfoils and described in his book,[7] was based on the minimum critical Reynolds number, and thus avoided having to introduce the disturbance level. It was Liepmann[56] who first worked out a formula that included most of the ingredients needed to use linear theory in transition prediction. This method can be classified as an amplitude density method, because it considers only a single frequency component, i.e., a single spectral line, from what must be a continuous disturbance power spectrum.

Liepmann's idea was that transition should occur when the ratio of the Reynolds stress of the boundary-layer disturbance equals the mean viscous stress, and that the linear theory provides an adequate means of computing the Reynolds stress. Liepmann's formula is

$$\frac{\tau'}{\tau} = -\frac{2}{c_f} \left\{ \left[\frac{\overline{u'v'}}{(\overline{u'^2}\ \overline{v'^2})^{\frac{1}{2}}} \right]_0 \left(\frac{\overline{v'^2}}{\overline{u'^2}} \right)_0^{\frac{1}{2}} A_0^2 \left(\frac{A}{A_0} \right)_{max}^2 \right\} , \qquad (91)$$

where c_f is the skin-friction coefficient. Liepmann used results of Schlichting[4,80] to evaluate all terms in (91) except the initial amplitude A_0. He believed A_0 to be related to the freestream turbulence level, but the details of this relationship are as unknown today as they were 30 years ago.

2. e^9 Method

The next step was the independent development by Smith and Gamberoni[53] and by Van Ingen[81] of what is often called the e^9 method. Smith and Gamberoni, starting from (91), found that the only quantity on the right-hand side that they could compute other than the skin friction, namely the amplitude ratio A/A_o, was itself sufficient to correlate a large number of experimental measurements of transition. With the use of the stability charts of Pretsch,[8] and an approximate method of computing the boundary layer developed by Smith,[82] transition was found to occur when $ln(A/A_o) \cong 9$. A similar result was obtained by Van Ingen, but with the exponential factor equal to 7 or 8. This method has been justly criticized for basing transition on a ratio and not on the disturbance amplitude. However, this criticism ignores the fact that the wind-tunnel data which were used to develop the method probably refer to rather similar disturbance environments, and also doesn't give credit to the value of the e^9 method in comparative studies. For a fixed value of A_o, which is equivalent to a fixed disturbance environment, the disturbance amplitude in the boundary layer does in large measure vary as A/A_o. Consequently, the effect on transition of changing a parameter which governs the mean boundary layer, such as the pressure gradient, can in this particular circumstance be estimated by means of the single factor A/A_o.

In more recent work, Jaffe, Okamura, and Smith[83] replaced the original approximate numerical methods of Smith and Gamberoni with more exact methods, and Van Ingen[84] widened the range of applications. However, the method remains essentially as originally developed, and the key to success still lies in a judicious choice of the value of the exponential factor. The use of the method is simplicity itself once the necessary numerical tools have been

assembled. Three computer programs are needed. The first computes the inviscid pressure distribution over a specified planar or axisymmetric body shape; the second uses this pressure distribution to compute the laminar boundary layer; and the third computes the spatial amplification rate and its integral, the amplitude ratio. Transition is considered to occur whenever $\ln(A/A_0)$ reaches the chosen numerical factor.

The only aspect of the method that remains to be mentioned is the equation for A/A_0. With a non-similar boundary layer, there is no simple relation between the arc length x^* and the boundary-layer thickness as with the Falkner-Skan profiles. One convenient expression is

$$\ln\left(\frac{A}{A_0}\right) = -\frac{U_\infty^* c^*}{\nu^*} \int_{x_0^*}^{x^*} \frac{(\alpha_i)_\delta^*}{R_\delta^*} \left(\frac{U_1^*}{U_\infty^*}\right) d\left(\frac{x^*}{c^*}\right) \ , \tag{92}$$

where c^* is the chord or body length, U_∞^* is the free-stream velocity, $U_1^*(x^*)$ is the edge velocity, R_δ^* is the local displacement thickness Reynolds number, and $(\alpha_i)_\delta^* = \alpha_i^* \delta^*$. As before, the integral is evaluated for a constant dimensional frequency. Another expression, which preserves the boundary-layer length scale $L^*(x^*) = [\nu^* x^*/U_1^*(x^*)]^{\frac{1}{2}}$, is

$$\ln\left(\frac{A}{A_0}\right) = -2 \int_{(R_\infty)_0}^{R_\infty} \alpha_i \left(\frac{U_1^*}{U_\infty^*}\right)^{\frac{1}{2}} d\, R_\infty \ , \tag{93}$$

where $R_\infty = (U_\infty^* x^*/\nu^*)^{\frac{1}{2}}$ and $\alpha_i = \alpha_i^* L^*$.

3. Modified e^9 Method

The main problem with the e^9 method lies in the proper selection of the exponential factor, which is by no means always equal to nine. One way to avoid an arbitrary choice is to relate the factor, which can be called n,

to the disturbance level in an empirical manner. This procedure has been applied to the case of freestream turbulence by Van Ingen[84] and Mack.[85] Wind-tunnel data on the influence of freestream turbulence on transition on a flat plate have been collected by Dryden[28] and are shown in figure 7. A more recent and more complete collection of data has been assembled by Hall and Gibbings,[88] but the additional data still follow the trend of figure 7. The start-of-transition Reynolds number is Re_t and the turbulence level is u_1'/U_1, or $T = [(\overline{u'^2} + \overline{v'^2} + \overline{w'^2})/3 \, U_1^2]^{\frac{1}{2}}$ if all three fluctuating velocity components have been measured. The turbulence level in a low turbulence wind tunnel is increased by successively removing the damping screens, and high levels are achieved by installing grids just upstream of the test section. The total disturbance level in a wind tunnel is made up of both turbulence and sound. Below $T = 0.1\%$, the sound component controls transition. As a result, decreasing the turbulence component only decreases the signal registered by a hot-wire anemometer without affecting the transition Reynolds number. It is for this reason that the curve in figure 7 is level for $T < 0.1\%$. The effect of freestream turbulence on transition is given by the sloping portion of the curve for $T > 0.1\%$.

An analysis of results computed from the stability theory shows that this portion of the curve can be accounted for by considering A to remain fixed at transition, and with

$$A_o \sim T^{2.4} \, . \tag{94}$$

This same variation in A/A_o is given by letting the exponential factor vary according to

$$n = - 8.43 - 2.4 \, \ell n \, T \, . \tag{95}$$

This method, where n is related directly to the disturbance level, may be called the modified e^9 method. Whether it is valid for other than flat-plate boundary layers cannot be determined until systematic transition data comparable to figure 7 become available for more general boundary layers.

C. Amplitude Method

1. Formulation of Amplitude Relation

Although the quantity A has been referred to in the foregoing as the amplitude, it is more properly called an amplitude density because we have been dealing solely with disturbances of a single frequency. That is, A represents only a single spectral line of a continuous power spectrum. The method of Liepmann, the e^9 and modified e^9 methods are all amplitude density methods. An amplitude density method which considers A to be a function of the energy density of the one-dimensional power spectrum of the external disturbance was developed by Mack[89] for transition in a supersonic wind tunnel. Although this method was reasonably successful in explaining the effects of Mach number, unit Reynolds number and tunnel size on transition, it can be criticized on the basis that a single spectral line is not an adequate basis for relating the disturbance spectrum in the boundary layer to the spectrum of the external disturbance source.

Consequently, another method has been developed which approximates the actual wide-band disturbance amplitude in the boundary layer. The starting point is the following expression for the disturbance amplitude A_d as a function of the Reynolds number $R = (U_1 x/\nu)^{\frac{1}{2}}$:

$$A_d^2(R) = \int_0^\infty d\left(\frac{\omega\Lambda}{U_1}\right) \int_{-\infty}^\infty A_o^2\left(\frac{\omega\Lambda}{U_1}, \beta\Lambda\right) \frac{A}{A_o}\left[\frac{\omega\nu}{U_1^2}, \beta\left(\frac{\nu x}{U_1}\right)^{\frac{1}{2}}; R\right]^2 d(\beta\Lambda). \quad (96)$$

In order to clarify the derivations, the use of asterisks has been dropped and all quantities are now dimensional except A, A_o and A_d which are referred to the freestream velocity. In (96), Λ is the length scale of the external disturbance, ω its (circular) frequency, and β its lateral wave number. The initial disturbance in the boundary layer is considered to be produced directly by the external disturbance and thus must be scaled in terms of Λ, while the amplitude ratio continues to be scaled in terms of the boundary-layer length scale. The velocity scale for both A_o and A/A_o is U_1. The basic assumption in (96) is that all phase relations are random so that the various harmonic components add in the square. Another viewpoint is that A_d is the long time average of the disturbance amplitude, and we will be determining the transition Reynolds number of this average disturbance. What we would really like to know is the average transition Reynolds number produced by a disturbance source that is steady only in its time average, and it is by no means certain that the two Reynolds numbers are the same.

It is entirely possible to evaluate the double integral of (96) numerically once A_o is known, but it is more prudent to adopt a simpler approach and keep the numerical requirements nearly the same as for the e^9 method. The two limiting cases which can be considered are where the bandwidth of the boundary-layer response is small compared to that of the external disturbance, and where the opposite prevails. We will treat only the first of these. Hence A/A_o acts as a δ-function and (96) can be written as

$$A_d^{\,2}(R) = A_o^{\,2}\left[\left(\frac{\omega\Lambda}{U_1}\right)_{max}, \; (\beta\Lambda)_{max}\right] \times$$
$$\int_0^{\infty} d\left(\frac{\omega\Lambda}{U_1}\right)\int_{-\infty}^{\infty} \frac{A}{A_o}\left[\frac{\omega\nu}{U_1^{\,2}}, \; \beta\left(\frac{\nu x}{U_1}\right)^{\frac{1}{2}}\right]^2 d(\beta\Lambda) \; . \tag{97}$$

We may further take advantage of che fact that the response curves A/A_o are often rather similar in shape, and evaluate the double integral in an approximate manner to arrive at

$$A_d^{\ 2}(R) = C_1^{\ 2} A_o^{\ 2}\left[\left(\frac{\omega\Lambda}{U_1}\right)_{max}, (\beta\Lambda)_{max}\right]\left(\frac{U_1\Lambda}{\nu}\right)^2 \frac{1}{R} \times$$

$$\frac{A}{A_o}\left[\frac{\omega\nu}{U_1^{\ 2}}, \beta\left(\frac{\nu x}{U_1}\right)^{\frac{1}{2}}\right]_{max}^2 \Delta\left(\frac{\omega\nu}{U_1^{\ 2}}\right) \Delta\left[\beta\left(\frac{\nu x}{U_1}\right)^{\frac{1}{2}}\right]. \tag{98}$$

The last two factors are consistently defined bandwidths of the frequency and lateral wavenumber response curves. The factors $(U_1\Lambda/\nu)^2$ and $1/R$ come from converting the integration variables $\omega\Lambda/U_1$ and $\beta\Lambda$ into the boundary-layer variables $\omega\nu/U_1^{\ 2}$ and $\beta(\nu x/U_1)^{\frac{1}{2}}$. The constant C_1 expresses the difference between the exact and approximate integrations.

2. Interaction Relation

In order to proceed further in the evaluation of A_d, it is necessary to relate A_o to the particular external disturbance under consideration. Unfortunately, at the present time nothing is known about the mechanism by which any external disturbance produces Tollmien-Schlichting waves. Although we could proceed on a purely empirical basis, a better appreciation of the problem is achieved by adopting a particular viewpoint. The viewpoint we adopt is that the instability waves are produced in the viscous sublayer, or Stokes layer, set up at the wall by the freestream disturbances. The forced response in this layer to a sinusoidal disturbance is obtained from the simplified model of Prandtl.[2] This approach was used by Sternberg[90] in studying the viscous sublayer of a turbulent boundary layer. The final step is to consider A_o to be proportional to the induced normal velocity of the forced response. The

idea of relating the free to the forced response had some success in studying supersonic boundary layers irradiated by strong acoustic disturbances.[91] A straightforward analysis leads to

$$
A_o^2 \left(\frac{\omega \Lambda}{U_1}, \beta \Lambda \right) = C_2^2 \left[\frac{1}{U_1} v_v' \left(\frac{\omega \Lambda}{U_1}, \beta \Lambda \right) \right]^2
$$

$$
= C_2^2 \left(\frac{\omega \nu}{U_1^2} \right) \left[\frac{p_\omega' (\omega \Lambda / U_1, \beta \Lambda)}{\rho U_1^2 \cos^2 \psi} \right]^2 , \tag{99}
$$

where v_v' is the rms normal "viscous" velocity of the harmonic component $(\omega \Lambda / U_1, \beta \Lambda)$, p_ω' is the corresponding rms pressure fluctuation at the wall, and ψ is the direction normal to the constant phase lines and cannot be near $90°$. The pressure fluctuation can be written more conveniently as

$$
\left[\frac{p_\omega' (\omega \Lambda / U_1, \beta \Lambda)}{\rho U_1^2} \right]^2 = \left(\frac{p'}{\rho U_1^2} \right)^2 F_2 \left(\frac{\omega \Lambda}{U_1}, \beta \Lambda \right) , \tag{100}
$$

where p' is the wide-band rms pressure fluctuation, and F_2 is a dimensionless two-dimensional spectrum function. A two-dimensional spectrum function is needed to account for the distribution of energy through different orientations for the same frequency. What is being said here is that a harmonic component $(\omega \Lambda / U_1, \beta \Lambda)$ of the freestream disturbance excites a Tollmien-Schlichting wave of the same frequency and orientation with an energy density proportional to the pressure-fluctuation energy density of the freestream component under the assumption that the imposed pressure fluctuation at the wall is the same as in the freestream. The proportionality factor is the dimensionless frequency $\omega \nu / U_1^2$, so that this line of reasoning has produced

the result that high frequencies are the most effective in producing insta-
bility waves. There is no cross spectral transfer of energy.

D. Effect of Freestream Turbulence on Transition

1. Application of Amplitude Method

In order to proceed further, we now restrict the freestream disturbance
to turbulence, and furthermore consider the turbulence to be isotropic. As
the pressure fluctuation appearing in (99) has been assumed to be the same as
in the freestream, isotropic turbulence theory[92] gives

$$\frac{p'}{\rho U_1^2} \propto \left(\frac{u_1'}{U_1}\right)^2 . \qquad (101)$$

Consequently,

$$A_o^2 \left(\frac{\omega \Lambda}{U_1}, \beta \Lambda\right) = C_3^2 \left(\frac{\omega \nu}{U_1^2}\right) \left(\frac{u_1'}{U_1}\right)^4 F_2 \left(\frac{\omega \Lambda}{U_1}, \beta \Lambda\right) \frac{1}{\cos^4 \psi} . \qquad (102)$$

As the x-Reynolds number does not appear in (102), we may take A_o to be the
amplitude at the neutral-stability point.

For a band of waves of the same frequency and different orientations,
the two-dimensional ($\beta = 0$) component will be the most amplified for fre-
quencies along the envelope curve of $\ln(A/A_o)$, i.e., the maximum $\ln(A/A_o)$ at
a given Reynolds number. These frequencies are given in figure 2 for the
Falkner-Skan profiles. The calculation of the lateral bandwidth $\Delta[\beta(\nu x/U_1)^{\frac{1}{2}}]$
in addition to $\ln(A/A_o)_{max}$, F_{max} and ΔF, involves the computation of four or
five times as many eigenvalues as are otherwise needed. Not enough numerical
results are available to make a general statement about the behavior of the

lateral bandwidth, but for the flat-plate boundary layer it decreases slightly with increasing R. For example, when defined, as is ΔF, as the $\Delta \beta$ at which Λ/A_o has decreased to $1/e$ of its maximum value, it is 0.109 at $R = 900$ and 0.081 at $R = 1600$. Since this change has little influence on the transition Reynolds number, we will proceed on the basis that the two-dimensional component is the most amplified and that the lateral bandwidth is constant. Consequently, the substitution of (102) into (98) yields, with this simplification,

$$A_d^2(R) = C^2 \left(\frac{U_1 \Lambda}{\nu}\right)^2 \left(\frac{u_1'}{U_1}\right)^4 \frac{1}{R} F_2 \left[\left(\frac{\omega \Lambda}{U_1}\right)_{max}\right] \times$$

$$\left(\frac{\omega \nu}{U_1^2}\right)_{max} \left[\frac{A}{A_o}\left(\frac{\omega \nu}{U_1^2}\right)\right]_{max}^2 \Delta\left(\frac{\omega \nu}{U_1^2}\right) . \tag{103}$$

The three quantities on the second line of (103) are all determined from stability theory. The first two of these are needed for the e^9 method, and the third is determined as explained in Section II-D.1 without having to do any extra eigenvalue computations.

The quantities in the first line of (103), except for R and the free constant C, are associated with the turbulence. It only remains to develop an expression for the spectrum function from isotropic turbulence theory. A convenient starting point is von Kármán's normalized (to 2π) interpolation formula[93]

$$E_1(k_1) = 4 \left[1 + \left(\frac{4}{3} k_1\right)^2\right]^{-5/6} \tag{104}$$

for the one-dimensional spectrum function of the longitudinal velocity component. The dimensionless frequency $\omega\Lambda/U_1$ has been replaced by the dimensionless

longitudinal wave number k_1 for the subsequent derivation. This procedure is permissible because all wave numbers k_1 have the convection velocity U_1. When Batchelor's theory[92] is applied to (104), a -7/3 rolloff is obtained for the one-dimensional pressure spectrum instead of -5/3 as in (104). A normalized interpolation formula equivalent to von Kármán's which has this behavior is

$$F_1(k_1) = 4 \left[1 + \left(\frac{5}{6} k_1 \right)^2 \right]^{-7/6} \tag{105}$$

The one-dimensional spectrum is given in terms of the three-dimensional spectrum by

$$F_1(k_1) = 2\pi \int_{k_1}^{\infty} k \, F_3(k) \, dk \ , \tag{106}$$

where $k = (k_1^2 + k_2^2 + k_3^2)^{\frac{1}{2}}$, and the two-dimensional spectrum is given in terms of the three-dimensional spectrum by

$$F_2(k_{12}) = \int_{-\infty}^{\infty} F_3(k) \, dk_3 \ , \tag{107}$$

where $k_{12} = (k_1^2 + k_2^2)^{\frac{1}{2}}$. Therefore,

$$F_2(k_{12}) = -\frac{1}{\pi} \int_{k_{12}}^{\infty} \frac{1}{(k^2 - k_{12}^2)^{\frac{1}{2}}} \frac{dF_1}{dk} \, dk \ . \tag{108}$$

An approximate evaluation of (108), which uses (105) and is correct for $k_{12} \gg 1$ and $k_{12} = 0$, is

$$F_2(k_{12}) = 1.78 \left[1 + (0.82 \, k_{12})^2 \right]^{-5/3} \ . \tag{109}$$

It may be observed that the rolloff in F_2 is -10/3 as opposed to -7/3 for F_1 and -5/3 for E_1. For use in (103) where $k_2(= \beta)$ is zero, k_{12} is replaced by $\omega\Lambda/U_1$. The two spectrum functions F_1 and F_2 are shown in figure 8. It may be observed that the integral of Γ_2 is equal to $F_1(0)/2$ as required by the above equations.

2. Numerical Results

All of the apparatus has now been assembled to make use of (103), but first the constant C must be evaluated. According to figure 7, $Re_t = 2.8 \times 10^6$ at T (or u_1'/U_1) = 0.001 for the flat-plate boundary layer, and with C = 1208 A_d = 0.04 at this Reynolds number for $R_\Lambda = U_1\Lambda/\nu = 4 \times 10^4$. In all subsequent calculations, C retains this value and transition is predicted to start whenever A_d first reaches 0.04. Any other value of A_d could have been chosen with a proportionate change in C.

It is easy to see from (103) that for given values of R and R_Λ, A_d varies as T^2, and A_d/T^2 thus defines a single cur .. There are two effects of the scale Reynolds number R_Λ which tend to oppose each other. The first effect increases A_d through the appearance of R_Λ as the proportionality factor relating the bandwidths referred to the boundary-layer scale length to the bandwidths referred to the turbulence length scale. Another way to look at this effect is that as the turbulence scale increases, the response curves spread over a greater frequency range of the turbulence power spectrum, with the result that more energy is included in the amplified band of frequencies and the transition Reynolds number is reduced. The second effect is that as R_Λ increases, the unstable frequency band, which is fixed in terms of $\omega\nu/U_1^2$ (cf. figure 3), moves to higher dimensionless frequencies $\omega\Lambda/U_1$ ($= F \cdot R_\Lambda$) with a smaller energy density and the transition Reynolds number is increased.

The only reported measurements on the effect of scale on transition[88] are

for turbulence levels between 1% and 3%, and show a marked increase in the

transition Reynolds number with an increase in scale. The amplitude method

gives a decrease of 16% in Re_t at T = 0.02% as R_Λ increases from 1×10^4 to

8×10^4 and the first effect prevails. At T = 1%, there is still a substantial

linear amplification region before transition, but this region is not necessarily

what is controlling transition. The Re_t of the amplitude method initially

decreases as R_Λ goes from 1×10^4 to 2×10^4, but then increases by 16% as R_Λ

increases further to 8×10^4 and the second effect prevails. This increase

is smaller, and Re_t higher, than in the experiment.

Disturbance growth curves for the flat-plate boundary layer are shown

in figure 9 for several turbulence levels. It is the steep slopes of these

curves which are the basic justification for the use of a method based on

linear stability theory for transition prediction. Figure 10 shows Re_t as

a function of T for six Falkner-Skan profiles, and the experimental flat-plate

data are repeated from figure 7. The theoretical curve given by the amplitude

method for $\beta = 0$ agrees well with these data for 0.09% < T < 0.27%. For

T < 0.09%, transition is controlled by sound, and agreement with the theory

is not expected. There is little point in being concerned about lack of agree-

ment elsewhere, because the experimental data to properly test the theory do

not exist at the present time. Only when enough data are available to make it

possible to sort out the effects of T and R_Λ will it be possible to say whether

the method given above properly accounts for the effect of freestream turbulence.

The curves in figure 10 for the other values of β give some idea of the

influence of a pressure gradient on transition. However, they cannot be used

for the prediction of transition in a real boundary layer on the basis of local

values of β, because Re_t depends on the amplification history of the disturbance.
Only if the particular value of β exists over a substantial portion of the
boundary layer, a situation most likely to arise fr. small favorable pressure
gradients, can figure 10 be expected to give a quantitative estimate of the
pressure gradient effect. Figure 11 is a crossplot of the results to show the
effects of β for several turbulence levels. The effect of T on Re_t is almost
independent of β for adverse pressure gradients, but for favorable pressure
gradients T has a progressively reduced effect as β increases.

It is of interest to know the value at transition of $\ln(A/A_o)_{max}$, i.e.
the e factor n, according to the amplitude method. In the e^9 method, n is of
course equal to nine for all boundary layers and all turbulence levels; in the
modified e^9 method n is given by (95) as a function of T for all boundary layers.
Only with the amplitude method is n a function of both T and the boundary layer.
As β decreases from $\beta = 0$ to -0.1 with $T = 0.1\%$, n decreases from 8.2 to 7.7;
as β increases to 0.2, n increases to 10.1. The effect of this variation in
n on Re_t is more clearly seen if we refer to the dashed curve in figure 11 of
the e^9 method. This curve is close to the $T = 0.05\%$ curve for $\beta < -0.05$, but
with higher values of β it departs more and more until at $\beta = 0.2$ it corresponds
to $T \sim 0.2\%$. Thus the amplitude method gives the result that turbulence levels
which vary by a factor of four can all give $n = 9$ at transition depending on
the value of β. Only experiments on pressure gradient boundary layers with
different turbulence levels can determine if the transition Reynolds number
really varies with T and β as given by the amplitude method.

The three methods of transition prediction which have been presented in
this section all use the same amount of computer time, because the eigenvalue
computations are what determine the time. Only if the lateral bandwidth for a

two-dimensional boundary layer is determined at each Reynolds number does
the amplitude method require substantially more time than the other two
methods. The amplitude method does have the disadvantage that a good
deal must be known about the disturbance source, but this is only a reflection
of the physical situation that transition is dependent on the type, intensity
and spectrum of the disturbance source, and not just on the boundary layer.
The method has been set up so that as information becomes available on the
mechanisms by which Tollmien-Schlichting waves are produced by external dis-
turbances, more realistic interaction relations can be easily incorporated
into the computer program. It is hoped that the development of a method which
may for the first time offer the possibility of a rational prediction of trans-
action will encourage the experimental work which is so necessary to arrive at
this long sought goal.

REFERENCES

1. Lord Rayleigh, On the Stability or Instability of Certain Fluid Motions, I, II, III, in "Scientific Papers," Vol. 1, pp. 474-484 (1880), Vol. 3, pp. 17-23 (1887), Vol. 4, pp. 203-209 (1895), Cambridge Univ. Press, London and New York.

2. L. Prandtl, Bemerkungen über die Entstehung der Turbulenz. Z. Angew. Math. Mech. 1, 431-436 (1921).

3. W. Tollmien, Über die Entstehung der Turbulenz. Gesellschaft der Wissenschaften, Göttingen, Math.-Naturwiss. Klasse, pp. 21-44 (1929).

4. H. Schlichting, Zur Entstehung der Turbulenz bei der Plattenströmung, Gesellschaft der Wissenschaften, Göttingen, Math.-Phys. Klasse, 181-208 (1933).

5. G. B. Schubauer and H. K. Skramstad, Laminar Boundary-Layer Oscillations and Transition on a Flat Plate, N.A.C.A. Report No. 909 (1948), N.A.C.A., Washington, D.C.

6. M. V. Morkovin, Critical Evaluation of Transition from Laminar to Turbulent Shear Layers with Emphasis on Hypersonically Travelling Bodies, Technical Report AFFDL-TR-68-149, Air Force Flight Dynamics Laboratory, Wright Patterson Air Force Base (1969), Ohio.

7. H. Schlichting, "Boundary Layer Theory," 6th Ed., McGraw-Hill, New York (1968).

8. J. Pretsch, Die Anfachung instabiler Störungen in einer laminaren Reibungsschicht, Jahrbuch der deutschen Luftfahrtforschung (1942). (Also N.A.C.A. Technical Memo. 1343, 1952.)

9. C. C. Lin, On the Stability of Two-Dimensional Parallel Flows, I, II, III, Quart. Appl. Math. 3, 117-142, 218-234, 277-301 (1945).

10. W. Reid, Uniform Asymptotic Approximation to the Solutions of the Orr-Sommerfeld Equation, Studies in Applied Mathematics 53, 91-110, 217-224 (1974).

11. W. B. Brown, Numerical Calculation of the Stability of Cross Flow Profiles in Laminar Boundary Layers on a Rotating Disk and in a Swept Back Wing and an Exact Calculation of the Stability of the Blasius Velocity Profile, Northrop Aircraft Inc., Report NAI 59-5 (1959), Los Angeles, Calif.

12. E. F. Kurtz, Jr. and S. H. Crandall, Computer-Aided Analysis of Hydrodynamic Stability, J. Math. Phys. 41, 264-279 (1962).

13. P. R. Nachtsheim, Stability of Free-Convection Boundary-Layer Flows, N.A.S.A. Technical Note D-2089 (1963), N.A.S.A., Washington, D.C.

14. W. B. Brown, Exact Numerical Solution of the Complete Linearized Equations for the Stability of Compressible Boundary Layers, Northrop Aircraft Inc., Norair Division Report NOR-62-15 (1962), Los Angeles, Calif.

15. L. M. Mack, Stability of the Compressible Boundary Layer According to a Direct Numerical Solution, AGARDograph 97, Part I, pp. 329-362, North Atlantic Treaty Organization (1965), Neuilly Sur Seine, France.

16. M. T. Landahl and R. E. Kaplan, Effect of Compliant Walls on Boundary Layer Stability and Transition, AGARDograph 97, Part I, pp. 363-394, North Atlantic Treaty Organization (1965), Neuilly Sur Seine, France.

17. A. R. Wazzan, T. T. Okamura and A. M. O. Smith, Spatial and Temporal Stability Charts for the Falkner-Skan Boundary-Layer Profiles, McDonnell Douglas Report No. DAC-67086 (1968), Long Beach, Calif.

18. H. J. Obremski, M. V. Morkovin and M. T. Landahl, A Portfolio of Stability Characteristics of Incompressible Boundary Layers, AGARDograph 134, North Atlantic Treaty Organization (1969), Neuilly Sur Seine, France.

19. A. R. Wazzan, T. T. Okamura and A. M. O. Smith, The Stability of Water Flow over Heated and Cooled Flat Plates, J. Heat Transfer 90, 109-114 (1968).

20. H. Schlichting, Enstehung der Turbulenz, in "Handbuch der Physik" (S. Flügge, ed.) Vol. VIII/I, pp. 351-450, Springer-Verlag Berlin (1959).

21. S. F. Shen, Stability of Laminar Flows, in "Theory of Laminar Flows" (F. K. Moore, ed.), pp. 719-853, Princeton Univ. Press, New Jersey (1954).

22. J. T. Stuart, Hydrodynamic Stability, in "Laminar Boundary Layers" (L. Rosenhead, ed.), pp. 629-670, Oxford Univ. Press, London and New York (1963).

23. W. H. Reid, The Stability of Parallel Flows, in "Basic Developments in Fluid Dynamics" (M. Holt, ed.), Vol. 1, pp. 249-307, Academic Press, New York (1965).

24. C. C. Lin, "The Theory of Hydrodynamic Stability," Cambridge Univ. Press, London and New York (1955).

25. R. Betchov and W. O. Criminale, "Stability of Parallel Flows," Academic Press, New York (1967).

26. A. S. Monin and A. M. Yaglom, "Statistical Fluid Mechanics: Mechanics of Turbulence" (J. L. Lumley, ed.), Vol. 1 (Chapter 2), The MIT Press, Cambridge and London (1971).

27. F. M. White, "Viscous Fluid Flow" (Chapter 5), McGraw-Hill, New York (1974).

28. H. L. Dryden, Transition from Laminar to Turbulent Flow, in "Turbulent Flows and Heat Transfer" (C. C. Lin, ed.), pp. 1-74, Princeton Univ. Press, New Jersey (1959).

29. I. Tani, Boundary Layer Transition, in "Annual Review of Fluid Mechanics," Vol. 1, pp. 169-196 (1969).

30. E. Reshotko, Boundary-Layer Stability and Transition, in "Annual Review of Fluid Mechanics," Vol. 8, pp. 311-349 (1976).

... M. V. Morkovin and L. M. Mack, High-Speed Boundary-Layer Stability and Transition, Recorded Lecture Series, Amer. Inst. Aeronautics and Astronautics, New York (1971).

32. M. Bouthier, Stabilité linéaire des écoulements presque paralleles, I and II, J. de Mécanique 11, 599-621 (1972), 12, 76-95 (1973).

33. W. S. Saric and A. H. Nayfeh, Non-Parallel Stability of Boundary-Layer Flows, Phys. Fluids 18, 945-950 (1975).

34. H. B. Squire, On the Stability of Three-Dimensional Disturbances of Viscous Flow between Parallel Walls. Proc. Roy. Soc. (London) A 142, 621-628 (1933).

35. L. M. Mack, A Numerical Study of the Temporal Eigenvalue Spectrum of the Blasius Boundary Layer, J. Fluid Mech. 73, 497-520 (1976).

36. D. Corner, D. J. R. Houston and M. A. S. Ross, Higher Eigenstates in Boundary-Layer Stability Theory, J. Fluid Mech. 77, 81-104 (1976).

37. G. B. Whitham, "Linear and Nonlinear Waves " Wiley-Interscience, New York (1974).

38. M. T. Landahl, The Wave Mechanics of Breakdown, J. Fluid Mech. 56, 775-802 (1972).

39. K. Stewartson, Some Aspects of Nonlinear Stability Theory, Fluid Dynamic Transactions, Vol. 7, Part 1, pp. 101-128, Polish Academy of Sciences (1975).

40. L. Lees, Instability of Laminar Flows and Transition to Turbulence, Consolidated Aircraft Corp. Report ZA-7-006 (1952), San Diego, Calif.

41. M. Gaster, A Note on a Relation between Temporally Increasing and Spatially Increasing Disturbances in Hydrodynamic Stability, J. Fluid Mech. 14, 222-224 (1962).

42. L. H. Thomas, The Stability of Plane Poiseuille Flow, Phys. Rev. 91, 780-783 (1953).

43. A. P. Gallagher and A. M. Mercer, On the Behavior of Small Disturbances in Plane Couette Flow, I, J. Fluid Mech. 13, 91-100 (1962).

44. S. A. Orszag, Accurate Solution of the Orr-Sommerfeld Stability Equation, J. Fluid Mech. 50, 689-703 (1971).

45. L. M. Mack, Computation of the Stability of the Laminar Compressible Boundary Layer, in "Methods in Computational Physics" (B. Alder, ed.), Vol. 4, pp. 247-299, Academic Press, New York (1965).

46. J. R. Radbill and E. R. Van Driest, A New Method for Prediction of Stability of Laminar Boundary Layers, North American Aviation, Inc.. AFOSR Report 66-0702 (1966), Downey, Calif.

47. L. H. Lee and W. C. Reynolds, On the Approximate and Numerical Solution of Orr-Sommerfeld Problems, Quart. J. Mech. Appl. Math. 20, 1-22 (1967).

48. A. Davey, A Simple Numerical Method for Solving Orr-Sommerfeld Problems, Quart. J. Mech. Appl. Math. 26, 401-411 (1973).

49. R. E. Kaplan, The Stability of Laminar Incompressible Boundary Layers in the Presence of Compliant Boundaries, Massachusetts Institute of Technology, ASRL-TR 116-1 (1964), Cambridge, Mass.

50. R. E. Bellman and R. E. Kalaba, "Quasilinearization and Boundary Value Problems," American Elsevier, New York (1965).

51. B. Antar, On the Solution of Two-Point Linear Differential Eigenvalue Problems, J. Comp. Physics 20, 208-219 (1976).

52. R. Jordinson and M. Gaster, On the Eigenvalues of the Orr-Sommerfeld Equation, J. Fluid Mech. 72, 121-133 (1975).

53. A. M. O. Smith and N. Gamberoni, Transition, Pressure Gradient and Stability Theory, Douglas Aircraft Company Report No. ES 26388 (1956), El Segundo, Calif.

54. M. Gaster, On the Effects of Boundary-Layer Growth on Flow Stability, J. Fluid Mech. 66, 465-480 (1974).

55. H. W. Liepmann, Investigations on Laminar Boundary-Layer Stability and Transition on Curved Boundaries, N.A.C.A. Advance Confidential Report 3H30 (Wartime Report W-107) (1943), N.A.C.A., Washington, D.C.

56. H. W. Liepmann, Investigation of Boundary-Layer Transition on Concave Walls, N.A.C.A. Advance Confidential Report 4J28 (Wartime Report W-87) (1945) N.A.C.A., Washington, D.C.

57. H. W. Bennett, An Experimental Study of, Boundary Layer Transition, Kimberley-Clark Corp. Report, Neenah, Wisconsin (1953).

58. H. L. Dryden, Air Flow in the Boundary Layer near a Flat Plate, N.A.C.A. Report No. 562 (1936), N.A.C.A., Washington, D.C.

59. F. X. Wortmann, Untersuchung instabiler Grenzschichtschwingungen in einem Wasserkanal mit der Tellurmethode, in "50 Jahre Grenzschichtforschung," pp. 460-470, Friedrich Vieweg, Braunschweig (1955).

60. F. N. M. Brown, The Organized Boundary Layer, Proceedings of the Sixth Midwestern Conference on Fluid Mechanics, pp. 331-349 (1959).

61. C. F. Knapp and P. J. Roache, A Combined Visual and Hot-Wire Anemometer Investigation of Boundary-Layer Transition, AIAA Journal 6, 29-36 (1968).

62. F. R. Hama, J. D. Long and J. C. Hegarty, On Transition from Laminar to Turbulent Flow, J. Appl. Physics 28, 388- (1957).

63. F. R. Hama and J. Nutant, Detailed Flow-Field Observations in the Transition Process in a Thick Boundary Layer, Proceedings of the 1963 Heat Transfer and Fluid Mechanics Institute, pp. 77-93, Stanford Univ. Press (1963), Palo Alto, Calif.

64. G. B. Schubauer and P. S. Klebanoff, Contributions on the Mechanics of Boundary-Layer Transition, N.A.C.A. Technical Note 3489 (1955), N.A.C.A., Washington, D.C.

65. P. S. Klebanoff and K. D. Tidstrom, Evolution of Amplified Waves Leading to Transition in a Boundary Layer with Zero Pressure Gradient, N.A.S.A. Technical Note D-195 (1959), N.A.C.A., Washington, D.C.

66. P. S. Klebanoff, K. D. Tidstrom and L. M. Sargent, The Three-Dimensional Nature of Boundary Layer Instability, J. Fluid Mech. 12, 1-34 (1962).

67. J. A. Ross, F. H. Barnes, J. G. Burns and M. A. S. Ross, The Flat Plate Boundary Layer. Part 3. Comparison of Theory with Experiment, J. Fluid Mech. 43, 819-832 (1970).

68. R. Jordinson, The Flat Plate Boundary Layer. Part 1. Numerical Integration of the Orr-Sommerfeld Equation, J. Fluid Mech 43 801-812 (1970).

69. N. Gregory, J. T. Stuart and W. S. Walker, On the Stability of Three-Dimensional Boundary Layers with Application to the Flow Due to a Rotating Disk, Phil. Trans. Roy. Sci. London 248(A), 155-199 (1955).

70. J. Laufer and T. Vrebalovich, Stability and Transition of a Supersonic Laminar Boundary Layer on an Insulated Flat Plate J. Fluid Mech. 9, 257-299 (1960).

71. B. Gebhart, Instability, Transition and Turbulence in Buoyancy-Induced Flows, in "Annual Review of Fluid Mechanics," Vol. 5, pp. 213-246 (1973).

72. A. Strazisar, J. M. Prahl and E. Reshotko, Experimental Study of the Stability of Heated Laminar Boundary Layers in Water, Case Western Reserve Univ., Dept. Fluid Thermal Aerospace Sci., Report FTAS/TR-75-113 (1975), Cleveland, Ohio.

73. P. S. Klebanoff and K. D. Tidstrom, Mechanism by which a Two-Dimensional Roughness Element Induces Boundary-Layer Transition, Phys. Fluids 15, 1173-1188 (1972).

74. M. Gaster and I. Grant, The Development of a Wave Packet in the Boundary Layer of a Flat Plate, Aeronautical Research Council, Fluid Motion Sub-Committee, A.R.C. 36 083, F.M. 4552 (1975).

75. J. M. Kendall, Wind Tunnel Experiments Relating to Supersonic and Hypersonic Boundary Layer Transition, AIAA Journal 13, 290-299 (1975).

76. T. Brooke Benjamin, Development of Three-Dimensional Disturbances in an Unstable Film Flowing Down an Inclined Plane, J. Fluid Mech. 10, 401-409 (1961).

77. W. O. Criminale and L. S. G. Kovásznay, The Growth of Localized Disturbances in a Laminar Boundary Layer, J. Fluid Mech. 14, 59-80 (1962).

78. M. Gaster, The Development of Three-Dimensional Wave Packets in a Boundary Layer, J. Fluid Mech. 32, 173-184 (1968).

79. M. Gaster and A. Davey, The Development of Three-Dimensional Wave-Packets in Unbounded Parallel Flows, J. Fluid Mech. 32, 801-808 (1968).

80. H. Schlichting, Amplitudenverteilung und Energiebilanz der kleinen Störungen bei der Plattenströmung, Gesellschaft der Wissenschaften, Göttingen, Math.-Phys. Klasse, Vol. 1, pp. 47-78 (1935).

81. J. L. Van Ingen, A Suggested Semi-Empirical Method for the Calculation of the Boundary Layer Transition Region, Univ. of Technology, Dept. of Aero. Eng. Report VTH-74, Delft, Holland (1956).

82. A. M. O. Smith, Rapid Laminar Boundary-Layer Calculations by Piecewise Application of Similar Solutions, J. Aero. Sci. 23, 901-912 (1956).

83. N. A. Jaffe, T. T. Okamura and A. M. O. Smith, Determination of Spatial Amplification Factors and Their Application to Transition, AIAA Journal 8, 301-308 (1970).

84. J. L. Van Ingen, Transition, Pressure Gradient, Suction, Separation and Stability Theory, Low-Speed Boundary-Layer Transition Workshop: II, Rand Corp., Santa Monica (1976).

85. L. M. Mack, On the Effect of Freestream Turbulence on Boundary-Layer Transition, Low-Speed Boundary-Layer Transition Workshop: II, Rand Cc Santa Monica, Calif. (1976).

86. A. A. Hall and G. S. Hislop, Experiments on the Transition of the Laminar Boundary Layer on a Flat Plate, Aero. Res. Comm. Reports and Memoranda 1843 (1938).

87. E. A. Wright and G. W. Bailey, Laminar Frictional Resistance with Pressure Gradient, J. Aero. Sci. 6, 485-488 (1939).

88. D. J. Hall and J. C. Gibbings, Influence of Stream Turbulence and Pressure Gradient upon Boundary Layer Transition, J. Mech. Eng. Sci. 14, 134-146 (1972).

89. L. M. Mack, A Numerical Method for the Prediction of High-Speed Boundary-Layer Transition Using Linear Theory, Proceedings of Conf. on Aerodynamic Analyses Requiring Advanced Computers, NASA SP-347, pp. 101-124 (1975). NASA, Washington, D. C.

90. J. Sternberg, A Theory for the Viscous Sublayer of a Turbulent Flow, J. Fluid Mech. 13, 241-271 (1962).

91. L. M. Mack, Linear Stability Theory and the Problem of Supersonic Boundary-Layer Transition, AIAA Journal 13, 278-289 (1975).

92. G. K. Batchelor, Pressure Fluctuations in Isotropic Turbulence, Proc. Cambridge Phil. Soc. 47, 359-374 (1951).

93. T. von Kármán, Progress in the Statistical Theory of Turbulence, J. Marine Research 7, 252-264 (1948).

	Spatial				Temporal			
Iter.	α_r	$\alpha_i \times 10^3$	c_{ph}	$\|\phi(0)\|$	α_r	$v_i \times 10^3$	c_{ph}	$\|\phi(0)\|$
0	0.1200	-5.0	0.250	0.189	0.1200	10.0	0.250	0.259
1	0.09421	-1.989	0.3184	0.0774	0.1048	-3.319	0.2861	0.157
2	0.09918	-3.453	0.3025	7.18×10^{-3}	0.1046	2.481	0.2869	0.0560
3	0.09964	-3.807	0.3011	5.29×10^{-6}	0.1001	1.223	0.2998	6.15×10^{-3}
4	0.09964	-3.811	0.3011	7.88×10^{-8}	0.1001	1.410	0.2996	5.38×10^{-6}
5	0.09964	-3.811	0.3011	8.83×10^{-8}	0.1001	1.412	0.2996	1.74×10^{-7}

Table I. Operation of Eigenvalue Search Procedure

$\beta = 0$, $R = 1000$, $F = 0.3 \times 10^{-4}$, NSTEP $= 80$, $y_1 = 8$, $\Delta = 0.001$

β	$\delta^* Re^{\frac{1}{2}}/x$	$\theta Re^{\frac{1}{2}}/x$	$\delta Re^{\frac{1}{2}}/x$	H	$U''(0)$	y_s/δ	c_s
1.0	0.6479	0.29234	3.1387	2.2162	-1.0000	-	-
0.5	0.9854	0.42899	4.3207	2.2969	-0.33333	-	-
0.2	1.3204	0.54770	5.2072	2.4108	-0.11111	-	-
0.1	1.4891	0.60024	5.5733	2.4809	-0.05263	-	-
0.05	1.5943	0.63044	5.7805	2.5289	-0.02564	-	-
0	1.7208	0.66411	6.0114	2.5911	0	0	0
-0.025	1.7950	0.68254	6.1389	2.6298	0.01235	0.1144	0.2178
-0.05	1.8790	0.70224	6.2771	2.6758	0.02439	0.1647	0.2999
-0.10	2.0907	0.74637	6.5994	2.8011	0.04762	0.2412	0.4018
-0.15	2.9149	0.79940	7.0385	3.0209	0.06977	0.3098	0.4650
-0.1988	3.4966	0.86811	8.2382	4.0279	0.09043	0.4216	0.5026

Table II. Properties of Falkner-Skan Boundary Layers

$$\beta = 0, \quad R = 1600$$

		Spatial				Temporal		
α_r	ω	$\alpha_i \times 10^3$	c_{ph}	ω_r	$\omega_i \times 10^3$	c_{ph}	c_g	$-\omega_i/\alpha_i$
0.08	0.0215	-3.458	0.269	0.0213	1.124	0.266	0.327	0.325
0.12	0.0351	-7.081	0.292	0.0350	2.499	0.292	0.359	0.353
0.16	0.0496	-2.890	0.310	0.0498	1.071	0.311	0.375	0.371
0.18	0.0578	3.566	0.321	0.0573	-1.345	0.318	0.369	0.377

$$\beta = -0.10, \quad R = 700$$

0.07	0.0201	-5.730	0.287	0.0196	2.060	0.280	0.358	0.360
0.13	0.0438	-13.71	0.337	0.0437	5.865	0.336	0.440	0.428
0.19	0.0719	-6.670	0.378	0.0726	3.532	0.382	0.537	0.530
0.25	0.1088	5.741	0.435	0.1081	-3.559	0.432	0.605	0.620

$$\beta = -0.1988, \quad R = 300$$

0.05	0.0134	-16.64	0.268	0.0104	5.645	0.208	0.337	0.339
0.19	0.0784	-42.42	0.413	0.0782	22.90	0.412	0.571	0.540
0.29	0.1331	-28.96	0.459	0.1372	16.78	0.473	0.601	0.579
0.41	0.2161	17.65	0.527	0.2103	-11.17	0.513	0.618	0.633

Table III. Comparison of Spatial and Temporal Theories for Three Falkner-Skan Boundary Layers

↓	R	F × 10⁴	↓	$\bar{\alpha}_i$ × 10³	α_i × 10³
0°	1600	0.30	0°	-3.82	-3.82
45°	2263	0.15	0°	-3.17	-3.17
			10°	-3.12	-3.07
			30°	-3.32	-2.88
			45°	-3.82	-2.70
60°	3200	0.075	0°	-2.46	-2.46
			10°	-2.42	-2.39
			30°	-2.59	-2.24
			45°	-2.98	-2.11
			60°	-3.82	-1.91
75°	6182	0.0201	0°	-1.37	-1.37
			10°	-1.36	-1.34
			30°	-1.49	-1.29
			45°	-1.75	-1.24
			60°	-2.32	-1.16
			75°	-3.82	-0.99

Table IV. Spatial Amplification Rates of Oblique Waves in the
Flat-Plate Boundary Layer for Different Values of $\bar{\Psi}$.
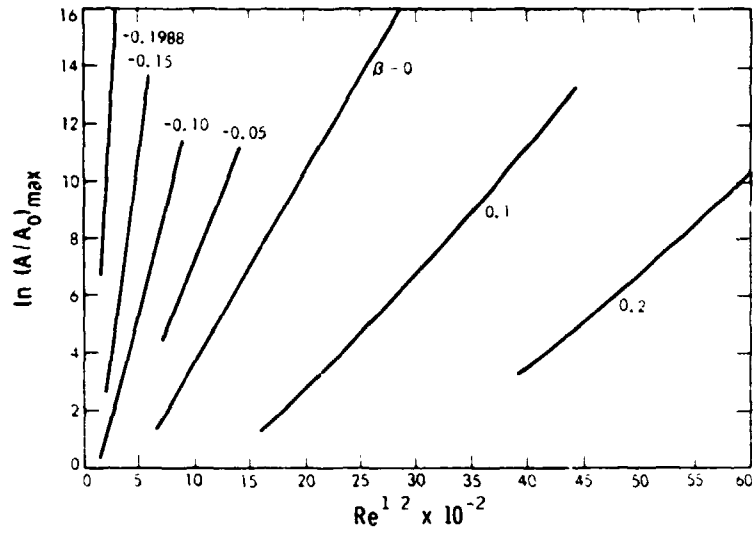
Figure 1.   Envelope curves of amplitude ratio
for Falkner-Skan boundary layers
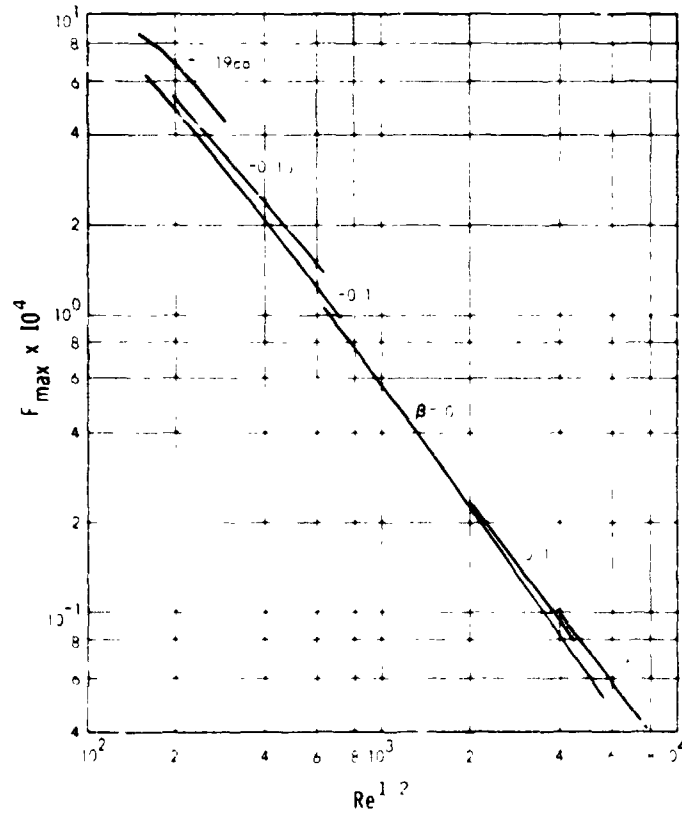
Figure 2.   Frequency of amplitude-ratio en-
velope curves for Falkner-Skan
boundary layers
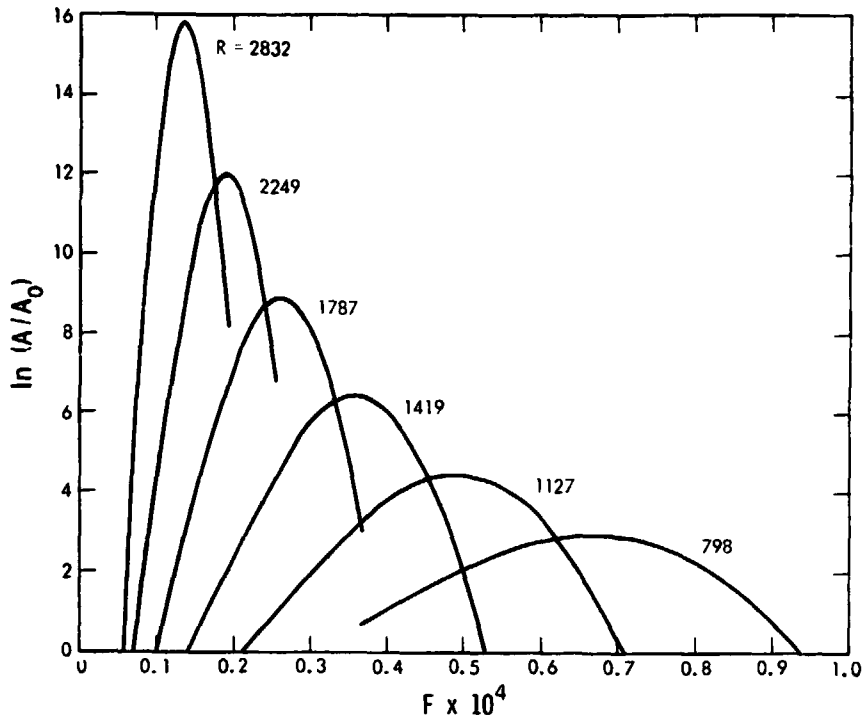
Figure 3. Frequency-response curves of amplitude ratio at several Reynolds numbers for flat-plate boundary layer
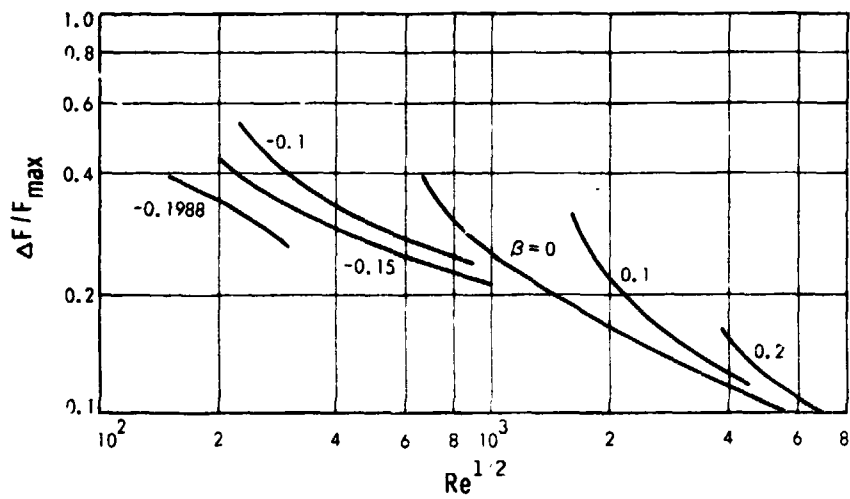
Figure 4. Reynolds number dependence of bandwidth of frequency-response curves for Falkner-Skan boundary layers
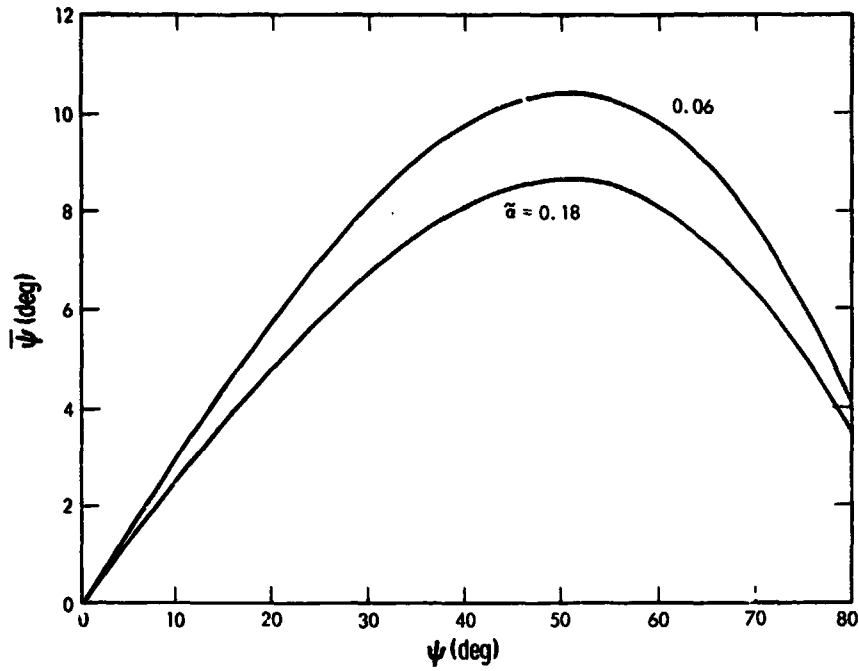
Figure 5. Direction of group velocity for oblique waves of constant wave number in flat-plate boundary layer, $Re^{1/2} = 1600$
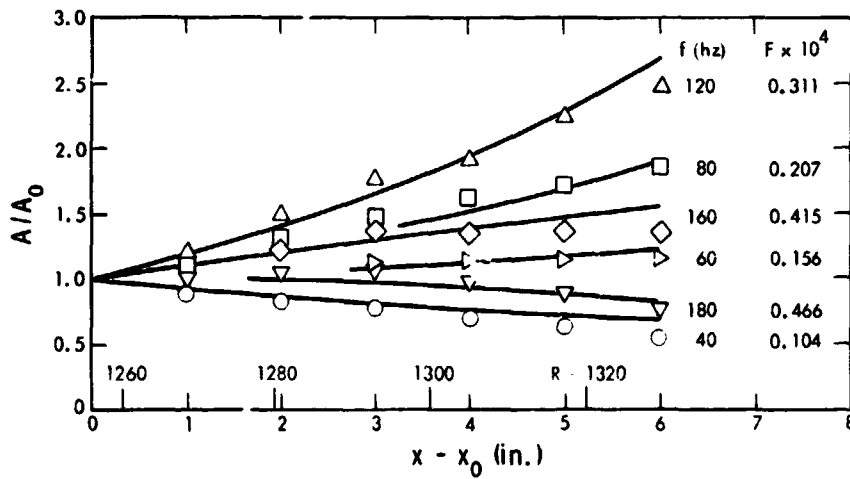
Figure 6. Comparison of theory with Schubauer-Skramstad measurements[5] of the growth of six constant-frequency waves in flat-plate boundary layer
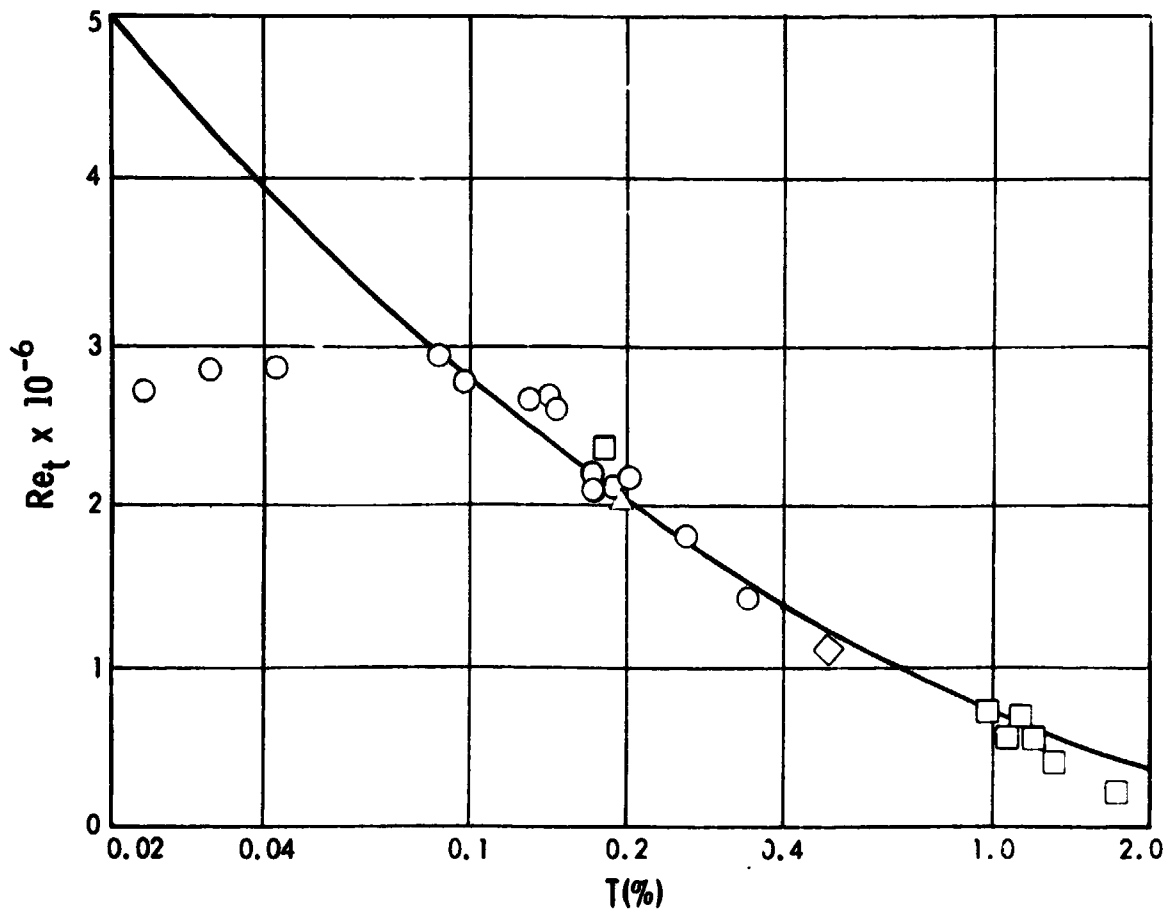
Figure 7.   Effect of freestream turbulence on the transition Reynolds num-
ber of the flat-plate boundary layer: o Schubauer-Skramstad[5];
□ Hall and Hislop[86]; △ Wright and Bailey[87]; ◇ Dryden[58];
—— modified e^9 method
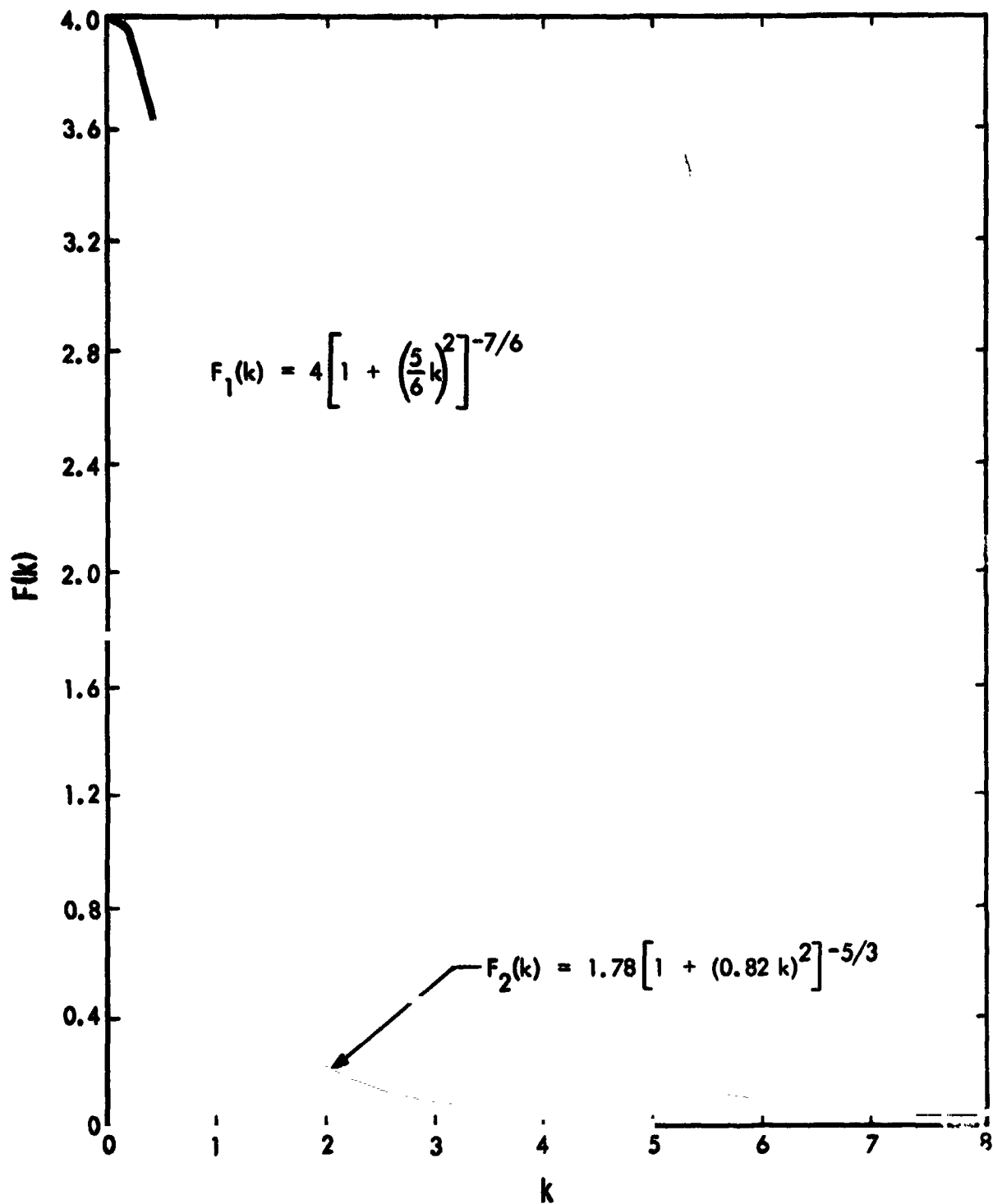
Figure 8. One- and two-dimensional interpolation pressure ectra of isotropic turbulence. F_1 is normalized to 2π
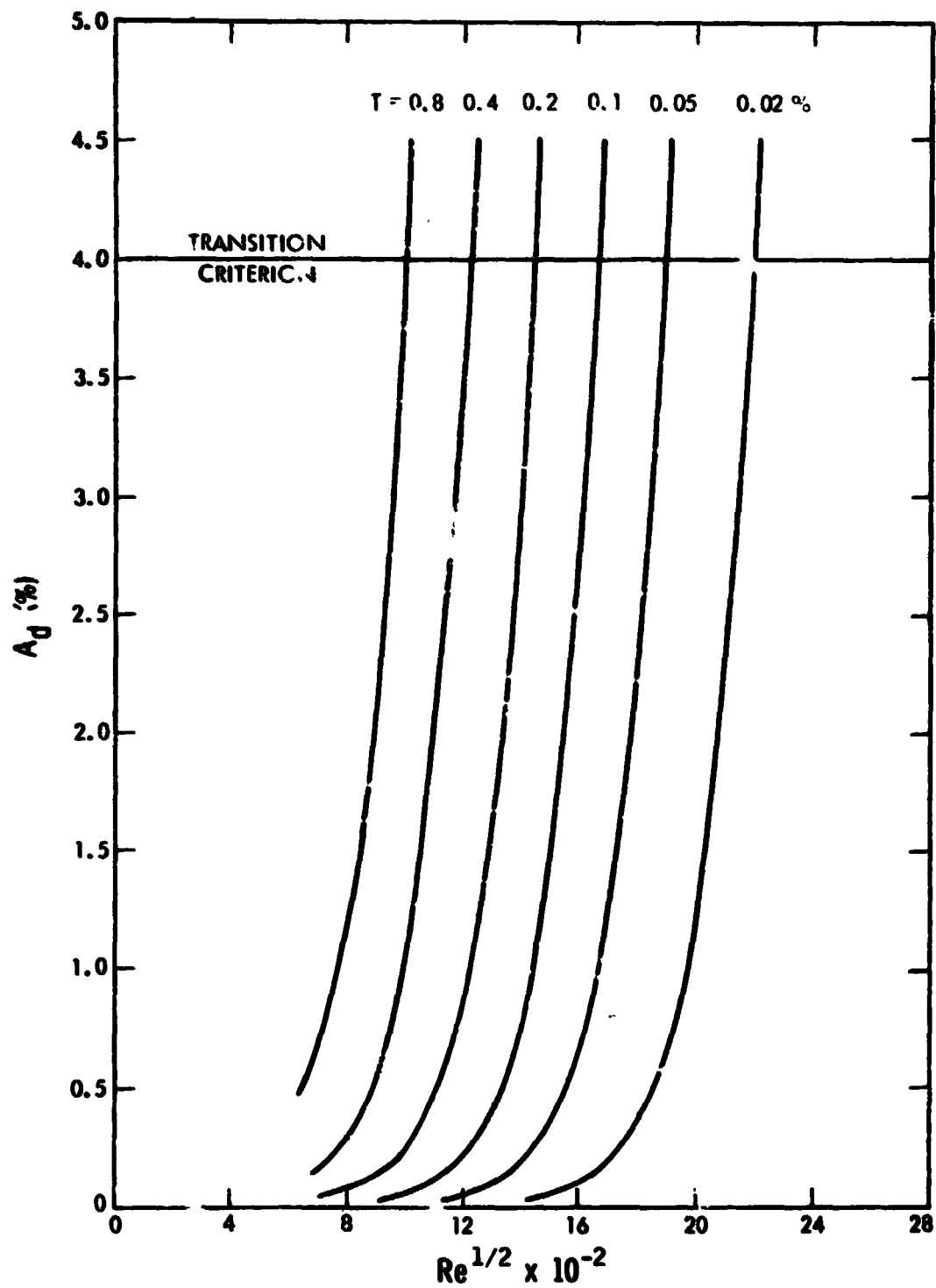
Figure 9. Disturbance amplitude growth in flat-plate boundary layer according to amplitude method for several freestream turbulence levels, $U_1 \Lambda / \nu = 4 \sim 10^4$
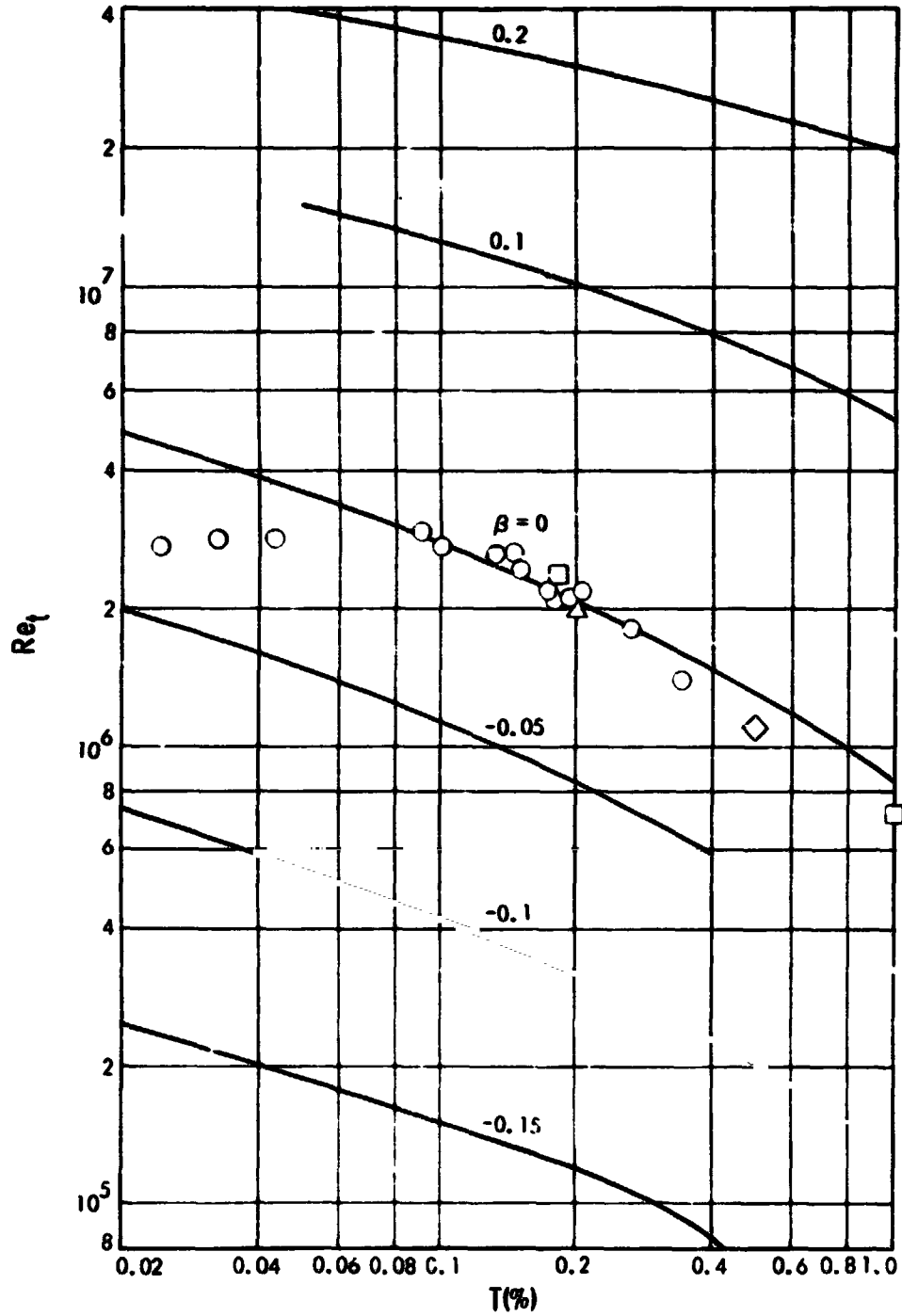
Figure 10. Effect of freestream turbulence on the transition
Reynolds number of Falkner-Skan boundary layers:
$U_1 \Lambda / \nu = 4 \times 10^4$; $\circ$, $\square$, $\triangle$, $\diamond$, experimental data
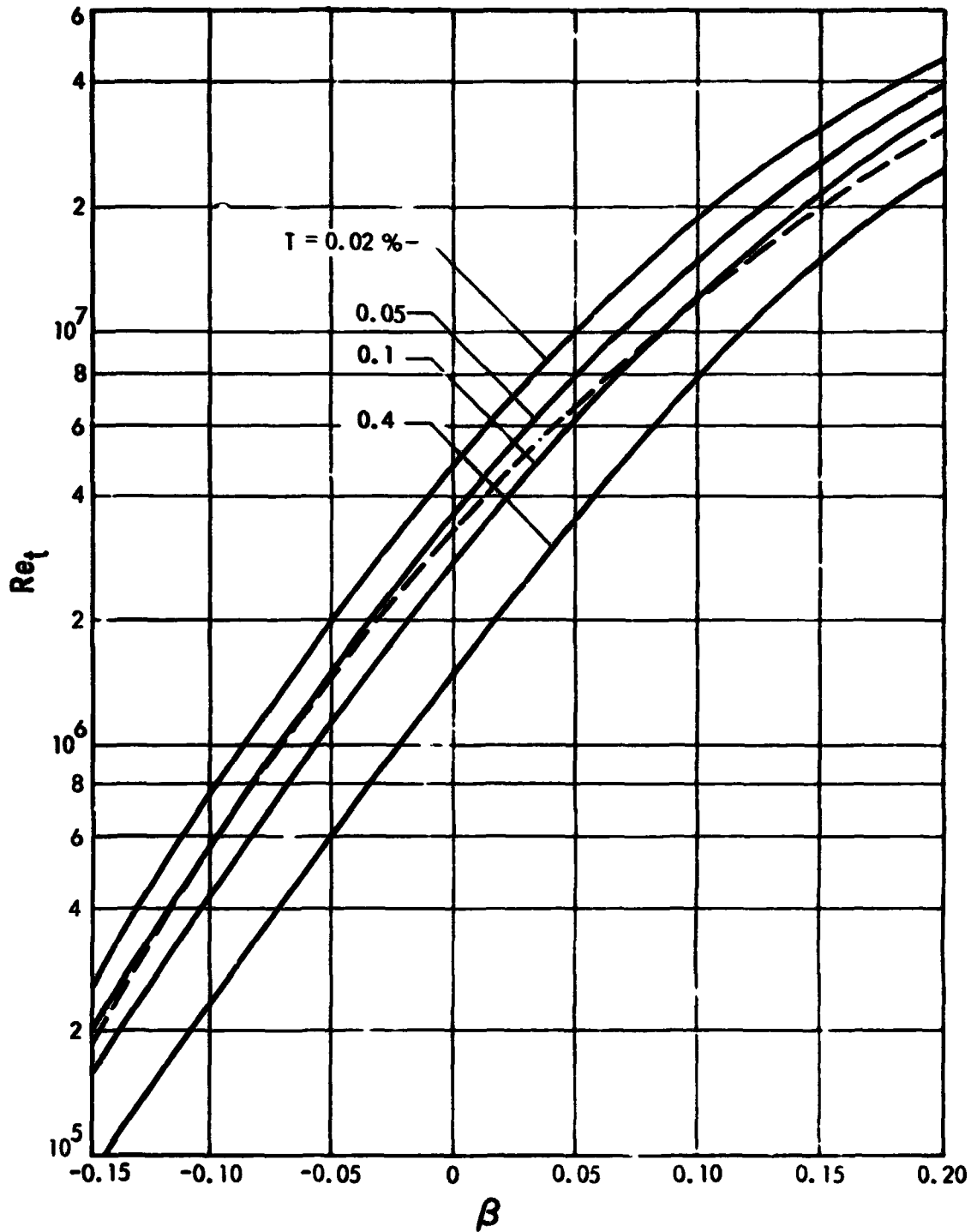(see caption of Figure 7 for sources); ———
amplitude method

Figure 11. Effect of pressure-gradient parameter on the transition Reynolds number of Falkner-Skan boundary layers according to amplitude method for four levels of freestream turbulence: $U_1\Lambda/\nu = 4 \times 10^4$; —— amplitude method: — — — e^9 method